DEVELOPMENT AND ASSESSMENT OF NON-DESTRUCTIVE EVALUATION TECHNIQUES FOR THE MEASUREMENT OF STRESS AND STRAIN IN BIOLOGICAL MATERIALS

BY

RYAN DAVID COULTER

A Thesis

Submitted to the Faculty of Graduate Studies

in Partial Fulfillment of the Requirements

for the Degree of

MASTER OF SCIENCE

Successfully Defended on April 23, 2007

Department of Biosystems Engineering

University of Manitoba

Winnipeg, MB, Canada

ABSTRACT

The heterogeneous and anisotropic nature of wood material creates additional design challenges not present with the use of other structural materials such as steel and aluminum. The natural variation in the physical properties of wood members requires that the specified strengths and resistances used for design calculations be based on the quantities measured for the fifth percentile of all wood materials tested. The result is that design may be unnecessarily conservative and subsequently inefficient.

The same properties that cause uncertainty surrounding the physical properties of biological materials also create difficulty in applying non-destructive evaluation techniques. Strain measurement is one particular technique that is extremely valuable for materials of known and consistent stress-strain relationships, but whose usefulness is diminished when applied to biological materials.

To demonstrate the need for more accurate strain measurement in light-framed structures, the predictive calculations and structural modelling of a post-frame building was compared to its demonstrated performance. The analysis did not adequately reflect the actual performance of the building, and it was determined that additional monitoring of light-framed buildings through systems such as strain measurement was required to gain a better understanding of the performance characteristics in order to optimize evaluation techniques.

This project aimed to develop a system that accurately measures strain in dimensional lumber of different types, which in turn will enable researchers to enhance monitoring the performance of light-frame structures and optimize design analysis and structural modelling techniques. The development of a methodology that provides a practical means by which to perform *in-situ* testing of post-frame buildings and decreases the complexity of post-frame building monitoring will contribute to the advancement of design and analysis techniques.

In the calibration phase of the project, metal foil resistance strain gages were mounted onto wooden specimens with dimensions of 5 x 13 x 40 mm, 5 x 40 x 100 mm, and 2 x 20 x 50 mm, and acrylic specimens with dimensions of 3 x 25 x 75 mm. These specimens were then subjected to loading in an ATS universal testing machine in the Physical Properties Lab at the University of Manitoba. Stress-strain curves were developed based upon the observed stress and strain levels. These calibrated gages were then mounted on to a 38 x 89 mm specimen of S-P-F dimensional lumber which represented a typical light-framed building material. This assembly was then subjected to a similar loading procedure as the calibrated gage and stress-strain curves were generated once again.

The slopes of the stress-strain curves developed from the two phases of the project were compared to determine if a consistent correlation existed. The three sizes of wood specimens did not demonstrate a consistent correlation. However, the acrylic specimen demonstrated consistent correlation amongst two groups of three with correlation

coefficients within a forty percent range in one group and within a nine percent range in the other group. This suggests that further experimental refinements could produce the desired results.

ACKNOWLEDGEMENTS

I would like to thank Dr. Kris Dick, my advisor for the patience and guidance that he has generously provided throughout the extended period of this research project. I also express my appreciation to Dr. Ron Britton and Dr. James Blatz, my thesis committee members whose experience and direction have increased the quality of this project.

A big thank you to Dale Bourns, Matt MacDonald, and Gerry Woods for their dedication, encouragement, and assistance in providing the lab space and research equipment and materials necessary for the successful completion of the project.

Manitoba Conservation, Manitoba Agriculture, Food, and Rural Initiatives, and the University of Manitoba also deserve thanks for providing me with the opportunity to complete the M.Sc. Program on a part time basis while maintaining full-time employment with the Provincial Civil Service.

Thanks also to Dave Coulter for his editing skills.

Finally, thanks to Van Doan for saying yes and keeping all of the promises we made on that one day in May.

TABLE OF CONTENTS

LIST OF FIGURES

LIST OF TABLES

LIST OF COPYRIGHTED MATERIAL FOR WHICH PERMISSION WAS OBTAINED

1.0 GENERAL INTRODUCTION

Modern structural design is based on an understanding of the physical properties of building materials and their performance when subjected to structural loads. For certain types of building material, like steel, these properties are thoroughly understood and the relationship between strain and stress is clearly defined. In other building materials, like wood, these relationships are based on a wider distribution of measured values, and therefore engineering designers are forced to deal with more uncertainties in structural design.

Strain measurement is a tool that has been used with great success in the 20th and 21st century for evaluating the physical effectiveness of structural materials. Using Hooke's Law, the stress of a member can easily be calculated from a measured strain within the elastic range. In the case of a material such as steel where its homogenous nature leaves little doubt regarding its physical properties, this calculation can be relied upon to provide accurate stress levels. However, in a heterogeneous and anisotropic material such as wood, the variation in physical properties between specimens creates an uncertainty regarding its physical properties, and therefore there is less confidence in the stress values calculated based on measured strain. The primary objective of this study is to develop a system that minimizes this uncertainty to an acceptable level for design.

Accurate strain measurement depends on the successful mounting of a strain gage to a test specimen. The accuracy necessary for the strain mounting procedure requires operator experience and the clean conditions of a laboratory. In the field, maintaining

chemically clean surfaces and precisely following the step by step procedures of strain mounting is difficult and there are many opportunities to introduce error into strain measurement. A system where the primary phase involves the delicate procedures of strain gage mounting in a lab setting, and where the second phase is to take the strain measurement materials developed in the lab to the field for strain measurement, has the potential to decrease the possible error sources and increase the reliability of strain measurement in the field.

The procedure evaluated in this research program is to apply a strain gage onto a small specimen of wood or acrylic and determine that specimen's stress-strain relationship. This specimen would then be attached to a piece of dimensional lumber and the stress-strain relationship would once again be measured. A consistent relationship between the stress-strain curves would provide the calibration coefficient necessary to apply the technology to field measurement.

With an established understanding of the structural performance of building materials in various applications, structural models can be developed that predict a building's structural behaviour. The exponential advances in software and computer technology have increased the usefulness and efficiency of structural modelling. Through the use of computers, more complicated structural models can be analyzed than was possible when the solution to the model relied on the expertise and physical labour of the design engineer. New and constantly improving structural modelling software is readily

available in today's marketplace and will continue to be a valuable tool for structural engineering design.

A structural model allows engineers to test the adequacy of proposed designs under expected loading conditions by reducing a structural system to its key components and connections. Since the accuracy and dependability of structural models is entirely based upon the input values of structural properties and performance characteristics, they are most useful for materials whose properties are thoroughly understood and reliable. For a building material such as wood where the physical properties such as modulus of elasticity (E) varies from one specimen to the next, it is prudent engineering practice to assign the lower E value to wood materials for the purposes of modelling. This is built into most models since the E value given to wood by design standards is based on the physical strength of the fifth percentile of tested members (Madsen 1992). The result of these safety factors is that structural modelling may produce an over-conservative design which reduces the economic efficiency of the building.

Non-destructive evaluation and real-time monitoring of buildings will allow a comparison of expected results produced by modelling techniques to the results measured through non-destructive evaluation techniques. In the case of light-framed buildings this non-destructive evaluation depends on the development of a system that is capable of accurately and precisely measuring the stress in its structural members. Where this system is in place its results can be compared to the results of a structural model, and

where necessary changes to the model can be made to make it more reflective of the structural performance of light-framed buildings.

The development of a specific technique for the measurement of stress and strain in wood structural members, and the optimization of structural modelling and non-destructive analysis of light-frame buildings will lead to an optimization of light-framed building structural design. This will enable enhanced safety and economy in the light-framed building industry, and will provide an opportunity for broader regulatory acceptance of alternative building designs, such as post-frame buildings.

2.0 GENERAL LITERATURE REVIEW

2.1 Introduction

An understanding of the physical properties of materials, including their strength and performance under load, has been a foundation of engineering and structural design for centuries. In his book *An Introduction to Natural Philosophy,* Denison Olmstead addressed this issue by stating *"The importance to the architect and the engineer of ascertaining the form and position of the materials which he employs, in order to secure the greatest degree of strength and stability at the least expense, has led mathematicians and writers on mechanics, to devote much attention to this subject"* (Archer and Lardner 1994). He goes on to state *"Strength is the power to resist fracture*." This paper will examine the physical properties of materials, the stress-strain relationship, strain measurement, strain gage technology, non-destructive testing, the science and art of structural modelling, and the basics of post-frame building design. Particular attention will be paid to the influence and application of these areas of structural engineering toward the stress evaluation of biological materials.

2.2 Physical Properties of Materials

A key concept in determining the strength of a material is understanding the relationship between stress (σ) and strain (ε) for that material, and subsequently its Modulus of Elasticity (E). The uniaxial normal stress of a material can be calculated when the internal forces acting on a specimen (P), and its cross sectional area (A) are known. Equation 2.1 illustrates this relationship.

$$\sigma = P/A$$ **Equation 2.1**

When subjected to a force or load, the length of the specimen will change. This displacement is depicted by the symbol δ. The relationship between this displacement, and the original length of the specimen as depicted in Equation 2.2, is known as strain (ε)

$$\varepsilon = \delta/L$$ **Equation 2.2**

Experimental evidence has shown that for linear elastic materials, a plot of stress-strain will result in a straight line whose slope, E, is known as its Modulus of Elasticity, or Young's Modulus (Archer and Lardner 1994). This is depicted by Equation 2.3, which can be rearranged into Equation 2.4, which is known as Hooke's Law (Khan 2001).

$$P/A = E\delta/L$$ **Equation 2.3**

$$\delta = \frac{PL}{AE}$$ **Equation 2.4**

Further rearrangement of Equation 2.4 is represented by Equation 2.5, which is also known as a one-dimensional Hooke's law for stress and strain.

$$\sigma = \varepsilon E$$ **Equation 2.5**

A uniaxial stress that produces a strain along the axis of the applied force will also produce a deformation and strain on the axis perpendicular to the applied force

(Khan 2001). These strains are related to each other by the constant μ, otherwise known as Poisson's ratio. Equation 2.6 depicts this relationship.

$$\mu = \varepsilon_x \Big/ \varepsilon_y \qquad \textbf{Equation 2.6}$$

Poisson's ratio is valuable as a means to calculate the shear modulus of a material through Equation 2.7

$$G = \frac{E}{2(1+\nu)} \qquad \textbf{Equation 2.7}$$

2.3 Strain and Strain Measurement

Two different kinds of strains need to be considered when studying the performance of axial structural members, normal strain and shear strain. Normal strain can be defined as the change in length of a line segment between two points divided by the original length of the line segment. Shear strain can be defined as the angular change between two line segments which were originally perpendicular (Dally 1965). Measurements of these strains are usually accomplished through the use of strain gages, types of which include mechanical, optical, acoustic, pneumatic, and electrical.

In 1938, Simmons at the California Institute of Technology, and Ruge at the Massachusetts Institute of Technology, independently discovered that small diameter wires made of electrical resistance materials could be adhesively bonded to a structure to measure its surface strain (Chalmers 1982). Prior to that, in 1856 Lord Kelvin reported that a difference in the tension of wire conductors affected their resistance properties.

This discovery led to the development of the bonded wire strain gage by Ruge and Simmons, which was later improved on with the introduction of the foil strain gage by Saunder-Roe Company in the UK in 1952 (Chalmers 1982). The foil strain gage is considered an electrical resistance type of strain gage, and they make up more than 80% of all strain gages used in experimental stress analysis conducted in the United States (Khan 2001).

2.3.1. Mechanical Strain Gages

Mechanical strain gages physically measure the change in length of a test specimen. Mechanical strain gages such as the Huggenberger gage must be physically attached to the test specimen by clamping its knife edges into the specimen. This is the major shortcoming of mechanical gages in that they have to be clamped with sufficient pressure so as not to slip during the test specimen's elongation, but also without so much pressure that the test specimen and gage will be damaged (Dally 1965). Mechanical strain gages have been mostly replaced by the electrical resistance strain gage and are now only used in special applications.

2.3.2 Optical Strain Gages

Optical strain gages also physically measure the elongation of a specimen, but rely on optics to amplify the change in length to a meaningful value. Optical strain gages include the Tuckerman optical strain gage. This gage operates on similar principles as the Huggenberger gage, but replaces mechanical levers with light rays for the magnification

of the displacement of the knife edges attached to the specimen (Dutton and Towle 1967).

2.3.3 Acoustic Strain Gages

Acoustic strain gages originated in the late 1920's, but have been largely displaced by electrical resistance gages (Dally 1965). The basic concept of acoustic strain gages is to adjust the acoustical frequency of a reference gage until no beats exist between its musical note and the musical note of the test gage. This produces a reading on a micrometer which forms part of the gage, which is in turn proportional to the strain of the test specimen. This type of gage has a limited range and is temperature sensitive, and requires a large force for operation. Alternate methods of acoustic strain measurement have recently been developed and will be explored further later in this thesis.

2.3.4 Pneumatic Strain Gages

Pneumatic strain gages were developed in the late 1930s by H. De Leiris, but are largely obsolete today (Dally 1965). In a pneumatic strain gage, air at a constant pressure is forced through an orifice where it strikes a top plate, and is horizontally deflected. There is a reservoir within the pneumatic strain gage that is maintained at a constant head, and a monometer whose head pressure is dependent on the airflow through the gage. When the gage is attached to a specimen experiencing longitudinal expansion or contraction, the distance from the air flow orifice to the top plate changes resulting in a change in manometer head. Since the head in the manometer is dependent on the deflection in the specimen, measurement of this head can be used to determine the strain level.

2.3.5 Electrical Strain Gages

Electrical resistance strain gages have been a powerful tool in experimental stress analysis since the late 1930's (Chalmers 1982). The performance and behaviour of strain gages has been steadily improving through time, and are often the basis of complicated measurement systems that rely on incredible levels of accuracy. Electrical resistance strain gages as small as 0.20 mm are commercially available (Khan 2001).

In addition to the electrical resistance strain gage which dominates the strain gage field today (Dally 1965), electrical strain gages also include the capacitance type and the inductance type. Similar to the mechanical and optical strain gages, the capacitance and inductance strain gages are attached to a test specimen with mechanical knife edges. This is a distinct disadvantage compared to the electrical resistance strain gage, and therefore these types of electrical strain gages are reserved for special applications (Dally 1965).

Electrical resistance strain gages work on the principle that all electrically conductive materials possess a strain sensitivity, that is to say that there is a ratio between the relative change of its resistance and a relative change in length (Chalmers 1982). An important property to consider when studying and using electrical resistance strain gages is the gage factor, or sensitivity. The resistance (R) of a uniform conductor with a length L, cross sectional area A, and specific resistance ρ is given by Equation 2.8

$$R = \rho L / A \qquad \textbf{Equation 2.8}$$

Strain sensitivity, or gage factor, F is given by equation 2.9

$$F = \frac{\Delta R / R}{\Delta l / l}$$ **; where**

Equation 2.9

$R = initial\ resitance$

$\Delta R = change\ in\ resistance$

$l = initial\ length$

$\Delta l = change\ in\ length$

Assuming the specific resistance ρ remains constant and incorporating Poisson's ratio, Equations 2.8 & 2.9 produce Equation 2.10 for the Gage Factor.

$$F = 1 + 2\nu$$ **Equation 2.10**

However, experimental evidence indicates that the assumption that specific resistance remains constant is invalid, and therefore Equation 2.10 is adjusted into Equation 2.11 to take into account the fact that the specific resistance, r, is affected by the strain.

$$F = (1 + 2\nu) + \frac{\delta r / r}{\varepsilon}$$ **Equation 2.11**

Electrical resistance strain gages can be further categorized into unbonded wire strain gages, bonded wire strain gages, metal foil strain gages, and weldable strain gages. In all

cases the strain gage consists of two primary components, the strain sensitive resistance element and the backing material. In order to achieve the necessary resistance levels the strain sensitive resistance element is typically placed in a zigzag pattern on the backing material so that the required length of wire or foil is concentrated in a small measurement area (Dally 1965).

2.3.5.1 Bonded Wire Strain Gage A typical bonded wire strain gage consists of approximately 10 cm of .002 mm diameter wire arranged in a grid pattern (Chalmers 1982). This grid of delicate wires is then sandwiched between two sheets of paper or other material in order to facilitate handling and mounting procedures, and to provide electrical insulation during use (Dally 1965).

2.3.5.2 Metal Foil Strain Gage Metal foil strain gages operate on the same principle as bonded wire strain gages, but instead of using small wires to construct the grid of the gage, thin foils of metal are photo etched into the required grid pattern and attached to the backing material. The photoetching process results in a rectangular cross section rather than the circular cross section found in wire strain gages (Chalmers 1982), which gives rise to benefits of foil strain gages over wire strain gages.

A significant advantage owing to the rectangular cross sectional area is that an increased amount of surface area is exposed or adhered to the applied force, therefore reducing the shear stress necessary to achieve the desired strain response (Chalmers 1982). This increased surface area contact allows for increased heat dissipation and therefore can

accommodate higher power levels which enable higher circuit sensitivities (Dally 1965). Figure 2.1 represents a typical metal foil strain gage and describes its different components. Terminal strips allow for a convenient soldering location for lead wires that eliminates the daunting task of soldering relatively large lead wires to the delicate strain gage.

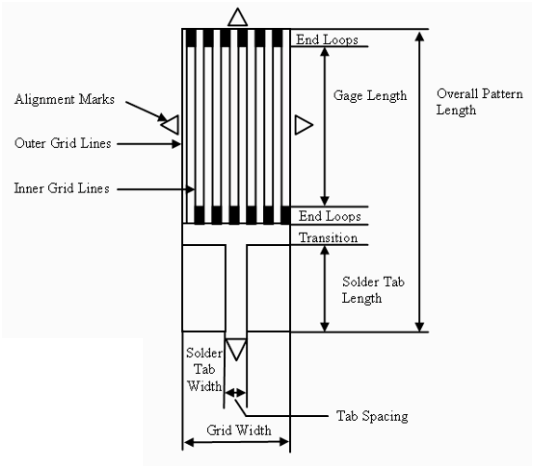

Fig. 2.1. A diagram of the components of a typical axial metal foil resistance strain gage

2.4 Strain Gage and Adhesive Selection

2.4.1 Gage Selection

Strain sensitivity as discussed earlier is just one of several factors to consider when selecting a material for electrical resistance strain gage. In order to satisfy the goal of combining an optimum electrical resistance material with a backing that consists of the desired manufacturing, utilization, and performance properties, several other factors need to be considered. These include size, durability, ease of production, repeatability and

linearity, cost, and resistance to hysteresis. These factors and their influence on gage performance are further discussed in section 2.6.

2.4.2 Adhesive Selection.

It is difficult to over emphasize the importance of the adhesive used in a strain gage assembly. Dally (1965) says that *"adhesive serves a very vital function in the strain-measuring system in that it must transmit the strain from the specimen to the gage sensing element without distortion."* Adhesives can affect all manners of strain gage measurements including gage factor, hysteresis, creep, and temperature effects. Chalmers (1982) lists the nine ideal properties of a strain gage adhesive as:

1. Capable of forming a thin, void free glue-line with high shear strength
2. Compatible with all gage backings, test materials and test surfaces
3. Capable of operating in all temperatures
4. Exhibit good linearity with minimum creep and hysteresis
5. Be a single part requiring no mixing
6. Require minimum curing time
7. Require no clamping
8. Have a long pot life
9. Capable of high elongation

While no single adhesive produced to date possesses all of the above listed properties, there are certain types that possess the necessary combination of properties to be suited for certain test conditions. In view of the fact that resistance strain gage theory assumes

that the strain gage is subjected to the same strain as the test specimen, it is extremely important to recognize the influence that the adhesive has on strain gage performance (Miles 1992).

Today's most commonly used adhesive types are cyanoacrylate, epoxy, and ceramic based adhesives (Khan 2001). Cyanoacrylate adhesives are generally useful for strain measurements less than three percent in temperatures between -185˚C and +95˚C. Cyanoacrylate is known to absorb water over time, and therefore the effectiveness of the bond is reduced as the test period extends. For this reason cyanoacrylate adhesives should only be used for applications of one year or less (Chalmers 1982).

Epoxy adhesives are generally used for strains between 3 and 15%. A disadvantage of epoxy over cyanoacrylate is that it requires two parts, a resin and a curing agent, which must be mixed to specified proportions. Khan (2001) states that a deviation of as little as 1% from the specified mixture recipe can influence curing temperatures and introduce stresses during polymerization of the epoxy compound.

2.5. Strain Gage Installation

Once the appropriate gage and adhesive have been selected, specific installation procedures must be followed. The installation process consists of the following major steps: planning, selection of installation material, preparation of test surface, gage preparation, application of adhesive, clamping, curing and post curing, lead wire attachment and soldering, application of protective coating, and verification of

installation (Chalmers 1982). The planning and selection steps have been previously discussed. The focus will now be on the remainder of the installation procedure.

2.5.1 Surface Preparation

Once all installation materials have been selected the surface of the test specimen must be prepared. This step is extremely important to the success of the strain gage installation (Procter 1977). Surface preparation requires solvent degreasing, abrading, application of gage layout lines, conditioning, and neutralizing (Chalmers 1982). Solvent degreasing removes contaminants from the surface of the test specimen and is the first step towards ensuring the chemically clean, neutral surface required for optimum performance of the gage. Abrading the surface to the required finish will improve the accuracy of the gage, and marking the gage location will make the installation process easier. However, marking the gage location usually introduces some level of contamination and therefore surface conditioning and neutralizing are required to return the surface to a neutral, chemically clean state (Chalmers 1982).

2.5.2 Application of Adhesive

Selection of adhesive used to install the strain gage is of fundamental importance. Strain gage theory relies on the assumption that the shear stresses are completely transmitted from the test specimen to the strain gage. An adhesive that is not capable of forming a thin, void free glue line with high shear strength, nor compatible with gage material will not allow for reliable operation of the gage. In addition, poor adhesives will significantly affect the performance characteristics of the gage including its gage factor, temperature

response, hysteresis and heat dissipation. Various types of adhesives are available, all with their own advantages and disadvantages.

2.5.3 Strain Gage Mounting

Once all of the preparation processes are complete, mounting of the strain gage onto the test specimen can be accomplished. It is important not to touch the electronic portions of the gage as this may lead to long term errors in resistance (Chalmers 1982). It is also important that the backing paper not be touched as this may lead to bonding problems. It is recommended that the gage be handled only with tweezers on the backing at a distance as far away from the foil as possible.

The typical mounting procedure is to position the gage and terminal strips in accordance with the gage layout lines, and place a piece of adhesive tape over the gage. The next step is to peel the tape partially off of the test specimen which lifts the gage up and exposes the underside of the gage for adhesive application. Keeping the tape anchored to one end of the test specimen during this step will ensure that the gage is returned to the desired position after the adhesive is applied. After applying the adhesive to the gage, the gage is repositioned to its desired position and the necessary clamping force is applied for a proper cure of the adhesive. Figures 2.2 & 2.3 illustrate these steps in the gage mounting process.

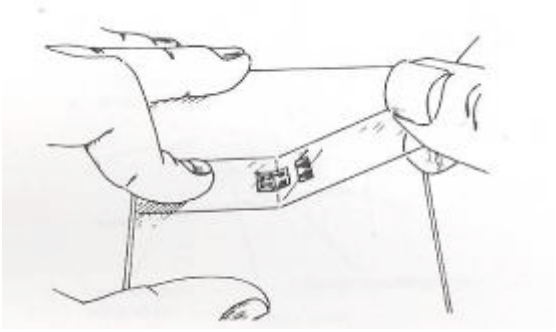

Fig. 2.2. Lifting the gage of the surface of the test specimen (Vishay 2005)
Used with permission from Vishay Micro Measurements, November 2, 2006

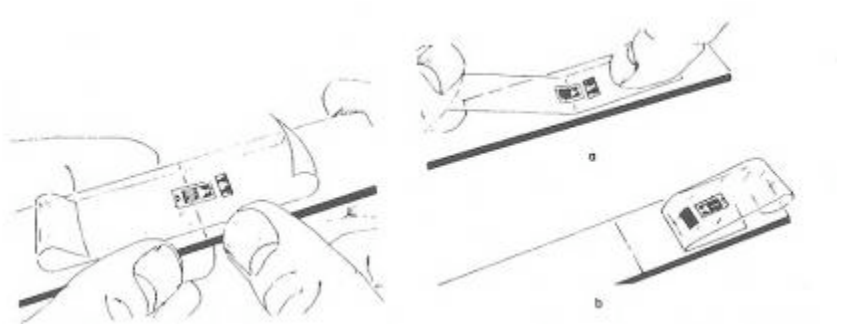

Fig. 2.3. Exposing the underside of the gage for adhesive application (Vishay 2005)
Used with permission from Vishay Micro Measurements, November 2, 2006

Once the adhesive has cured and the gage has been properly mounted to the test specimen, jumper wires are soldered from the foil to the terminal strips, and lead wires are soldered to the terminal strips. These lead wires are then connected to measurement equipment and testing can begin.

2.6 Error Sources in Strain Measurement

2.6.1 Operational Parameters

The operation of strain gages depends on certain performance characteristics that are important to understand when undertaking the gage selection process. The gage factor

and transverse sensitivity should be considered, as well as temperature effects, elongation capability, fatigue life, operating temperature range, linearity, hysteresis and zero shift.

Hysteresis refers to a delayed response in a material undergoing cyclical loading, where its internal stress level has a certain level of dependence on its recent stress history. In other words, there is a delayed response in the substance during cyclical loading that will result in slightly different strain readings at a specific stress level in cyclical loading. In the case of strain gages, hysteresis can be a significant source of error and over time may lead to zero shift in strain cycling. Esin (1980) describes this hysteresis loop as an inelastic behaviour under cyclic loading.

Linearity refers to the fact that no material is perfectly linear throughout all operation conditions. However, most modern strain gages show linearity throughout their operating conditions. Zero shift is directly related to the hysteresis effect and refers to strain level not returning to zero when the applied stress, or force, is removed. Over numerous cycles an accumulation of these zero shifts requires consideration (Khan 2001).

Linearity, hysteresis, and zero shift are functions of the strain sensing element, the backing material, the strain level, and the adhesive cure. In a properly installed strain gage the effects of these factors are negligible and do not require a correction to be applied (Chalmers 1982).

Gage factor variations with temperature changes are presented in Figure 2.4. It is evident from this figure that for certain materials and certain temperature ranges this variation in sensitivity can be safely neglected, while in others it is extremely important to note. One cause for this change in gage factor is the differential expansion and contraction of the strain sensing element and the backing material of the strain gage (Khan 2001). This introduces a certain amount of strain into the system that depending on the time frame and temperature deviation could be extremely detrimental to the test program if not adequately compensated for.

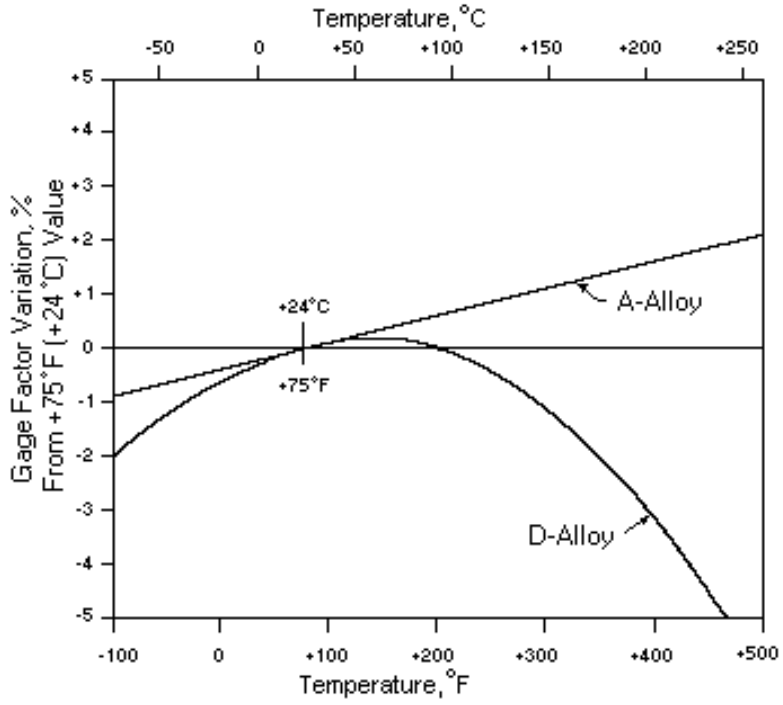

Fig. 2.4. Gage factor variance with temperature for constantan and isoelastic gages (Vishay 2007) Used with permission from Vishay Micro Measurements, May 7, 2007

Another temperature effect to consider is the change in resistance with temperature of the alloys used in strain gages. For example, the resistance of a copper-nickel alloy varies by

a linear value of approximately 1% per 100˚C (Chalmers 1982). In some circumstances this change in resistance with temperature can be used to offset the induced strain resulting from differential expansion of gage materials and therefore eliminating the temperature effect. These types of gages are referred to as self-temperature compensated (STC) gages (Khan 2001).

Acceptable and reliable performance of strain gages also requires sufficient heat dissipation. In the case of a strain gage applied to a poor heat sink, such as a plastic or organic test specimen, hot spots may develop in the gage grid that can alter the elastic modulus of the test specimen and produce erroneous results (Chalmers 1982).

2.6.2 Physical Parameters

Sources of error related to the physical operation of the gage include gage elongation, stress relaxation in the adhesive and metal fatigue. All gages have a maximum elongation that can be managed, which if exceeded will result in physical and permanent damage to the gage. Prolonged and cyclical loading can also result in creep and stress relaxation in the gage adhesive, therefore reducing the transmission efficiency of stress on the surface of the test specimen to the gage itself (Khan 2001). As with all metals, electrical resistance strain gages eventually fail in fatigue due to prolonged and repeated loading cycles (Chalmers 1982). In wire gages this results in an open circuit, whereas in metal foil gages small cracks will form across the cross section of the grid which increases the resistance, and produces a positive zero shift in the strain gage readings. The opening and closing of these cracks also results in a change in resistance that is not

relative to the normal resistance changes due to strain. This phenomenon is known as super-sensitivity.

Strain gage misalignment can also cause serious errors in strain measurement (Miles and Tanner 1992). In a study examining the thrust on a shaft subjected to a torque to thrust ration of 7.5:1, a misalignment of one degree led to an error of 53% in the strain measurement.

Humidity and moisture can also affect gage performance by degrading the adhesive bond and reducing the gage to ground resistance (Khan 2001). In certain circumstances hydrostatic pressure, thermal EMFs and magnetic fields can also be produced which will have detrimental effects on the accuracy of strain gage measurements.

2.7 Instrumentation and Strain Measurement

The strain gage itself is just one component of the system that is required in order to obtain reliable strain measurement. These systems typically consist of a power supply, a wheatstone bridge circuit, an amplifier, a computer or processor, and some type of display. The power supply provides a means to deliver voltage to the strain gage in order that changes in resistance can be measured.

A wheatstone bridge is a circuit consisting of four resistors, at least one of which is the strain gage measuring strain in the test specimen, which makes it possible to measure small resistance changes in the strain gage (Dally 1965). These resistance changes in the

strain gage cause an out-of-balance voltage that is measured by the wheatstone bridge, and is amplified and stored in a usable format (Owens and Scott 1982). The means by which a wheatstone bridge converts a small change in resistance to an amplifiable voltage are explained by Figure 2.5 and the associated equations.

In Figure 2.5; if $R_1/R_3=R_2/R_4$, the wheatstone bridge is considered to be balanced and the voltage output will be zero. If there is a change in resistance in one of the resistors, for example a strain gage, then the bridge becomes unbalanced and there will be an output voltage in accordance with Equation 2.12

$V_{out} = F\varepsilon NV_{in}/4$; where **Equation 2.12**

F = *gage factor*

V_{in} = *bridge volts*

N = *number of active bridge arms*

This output voltage can be directly measured and converted to a strain amount.

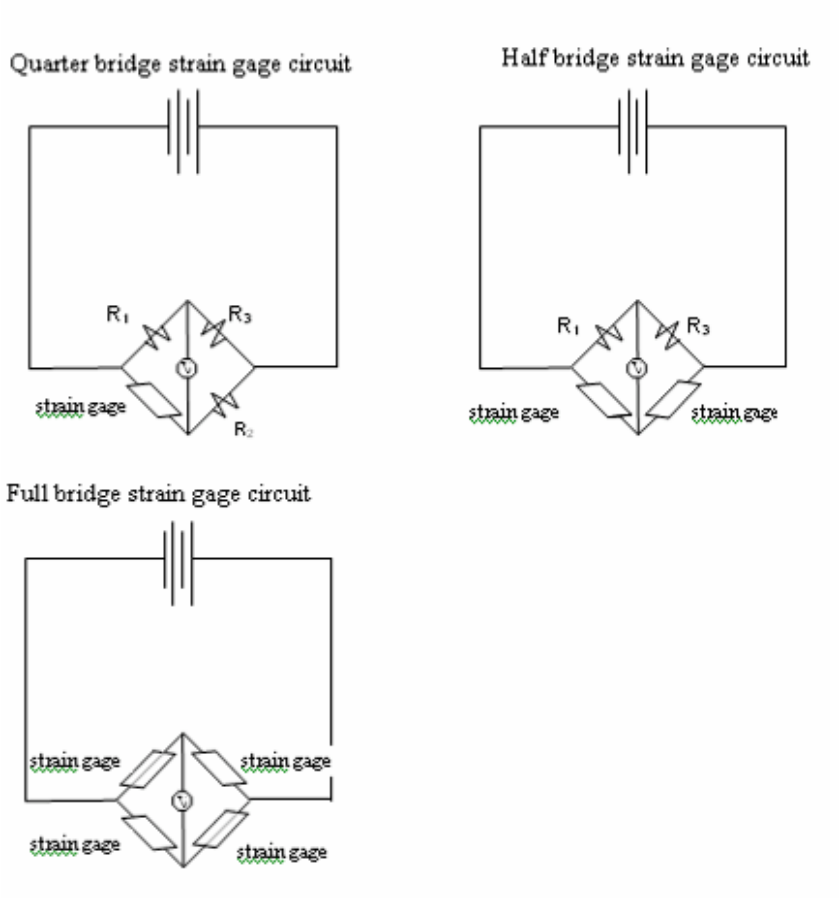

Fig. 2.5. Schematics of the various wheatstone bridge configurations

When all four bridge arms are active, it is known as a full wheatstone bridge, when two arms are active it is known as a half bridge, and when only one active bridge arm is used, it is known as a quarter bridge. A bridge arm is active if it consists of a strain gage undergoing deformation and being used for strain measurements. Different configurations of the wheatstone bridge can be used to compensate for introduced errors in strain measurement.

For example, in a full wheatstone bridge, a 'dummy gage' exactly the same as the active gage can be used in one of the inactive arms and placed on an unstressed portion of the

test specimen in close proximity to the active gage. In this scenario, any induced stress resulting from temperature effects is eliminated when the effects on the two gages cancel each other out (Dally 1965).

The voltage output from the wheatstone bridge is amplified and converted to a strain value that is either displayed, or stored. When all components of the strain measurement system are working properly, strain gage measurements can be easily accomplished.

2.8 Strain Measurement in Biological Materials

Through the equations presented in Section 2.2, it is possible to calculate the stress of a test specimen based on known physical properties and measured physical values, such as physical elongation. Young's modulus is fairly constant for relatively homogeneous materials such as most metals, and therefore calculations can proceed with sufficient accuracy. However, for non-homogenous or composite materials such as wood or bones, the range of Young's modulus between different specimens may be too large to provide sufficient confidence in their accuracy. Destructive testing is therefore usually necessary to determine the actual physical strength of each specimen of a material such as wood, which is an unrealistic scenario. Because it is not feasible to strength test each specimen of biological material destined for use in a structure, it has been accepted that the allowable stress be considered that of the weakest 5% of tested materials
(Canadian Wood Council 1995), and Limit States design demands additional safety factors throughout the calculations.

As a result, buildings such as light-framed wood structures that use non-homogeneous and anisotropic materials may be constructed in a manner such that there is not the ideal balance between their strength and cost, the balance that Olmstead (Archer and Lardner 1994) states all engineers and architects strive for. Therefore, it is necessary to examine other monitoring and design techniques additional to those that traditional structural engineering has developed for typical building materials such as steel. Non-destructive testing is an important method of accomplishing this, and also opens up the possibility of studying the performance of structural members in real time and *in-situ*. This in turn will allow for the review of established design methods with the possibility of changing building codes and assumed performance characteristics in an effort to optimize engineering design.

While strain measurement in biological materials is less of an exact science than traditional strain measurements, the variables affecting installation and the possible sources of error are similar (Miles and Tanner 1992). Of particular note is the stiffening effect that a gage may have on a low elastic modulus material. Even with a well defined material such as brass, studies have shown that strain gage readings vary by as much as 20%. The calibration of strain gages is essential in order to provide confidence in the data obtained.

2.9 Non-destructive Evaluation

2.9.1 Non-destructive Evaluation Using Strain Gages

The value of strain gages in the field of stress analysis extends beyond their use as a distinct strain measuring technique. Due to some of the difficulties associated with correctly using strain gages and the many possible error sources, researchers have developed alternate methods of strain measurement as detailed in the following sections. In many cases, these methods are validated through a comparison with the results yielded from traditional strain measurement. For example, Margetson (1981) set out to develop an empirical equation to approximate the stress-strain characterization of non-linear materials. By comparing the results of his calculations to the measured experimental results obtained from strain gage measurement, Margetson (1981) was able to conclude that his formula was appropriate for predicting stress levels.

Strain gages were also used by Soden and McLeish (1976) to determine the strength of Balsa wood. Experimental treatments using a loading machine determined the failure stress of different specimens of balsa wood cut in varying angles related to the grain. It is the function of strain gages within the test apparatus that determines the stress applied to the test specimen and enables us to determine the stress allowance in various materials. Measurement of stresses during construction of the Milford Haven Bridge in Wales were accomplished with strain gages (Beales and Cullington 1977) and enabled the researcher to determine what aspects of construction influenced or created stress in the bridge members. This understanding of the properties and performance of a structure are

important to the design engineer who is responsible for ensuring that the materials, design and construction proposed are adequate for the applied loads.

When performing stress analysis with strain gage equipment, it is important to have an understanding of where on the test specimen the critical stress will occur (Miles and Tanner 1992). Analysis techniques, such as using the least squares method to address errors between gage measurements (Lightfoot and Randolph 1975) can be used to refine various models, but the most effective method is to identify the appropriate test location in the first place.

Direct strain measurement using electrical resistance strain gages has been a common non-destructive health monitoring technique for many disciplines of engineering. The eloquence of the strain gage provides a unique opportunity to study the behaviour of structural members and determine the strength of a structure. Elazaby and Simmonds (1992) state that for reinforced concrete sections, the relationship between axial force, bending moment and curvature can be calculated based on known stress-strain relationships for concrete and steel. Strain gages have also been employed in research projects of which the focus was testing new construction or control techniques.

For example, Mahadzer et al. (1998) were interested in determining the application of geotextile strips as reinforcement on soil slopes. In their experiment, strain gages were used to measure the tensile strain in a geotextile under simulated conditions. Based on

the measurements of this study, the authors concluded that the proposed method for stabilizing the slope was acceptable.

The phenomenon of residual stresses and stress relaxation is another to which strain gage performance and properties have proven valuable for research. In order to gain a more thorough understanding of stress relaxation in welded steel plates, strain gages were used to measure the change in strain when residual stresses were relieved by an external operation. In this case, stress was introduced into the specimens by the welding process, after which strain gages were mounted (Chance and Bray 2002). The researcher then relieved the residual stress in the welded steel plates at different time intervals by cutting through the welded portion of the plates. Measurement of the stress relaxation could then be taken from the strain gages. Strain gage technology enabled Chance to determine that there is indeed a measurable, predictable, and time dependent stress relaxation in welded steel plates.

2.9.2 Alternate Methods of Strain Measurement in Non-destructive Evaluation

Additional methods beyond strain gage methods have been proven effective in the field of non-destructive health monitoring. The following is a summary of some of the other non-destructive evaluation techniques that have been developed.

2.9.2.1 Piezoelectric Sensors Martin et. al. (2002) attempted to simulate the nervous system of the human body for structural health monitoring of a large structure. Rather than using strain gages, Martin (2002) used an array of piezoelectric sensors to measure

acoustic emissions and dynamic strains throughout a structure. This type of monitoring system is becoming necessary because traditional metals are being replaced by composite materials, which at times have shown unpredictable behaviour and do not follow traditional stress models. A properly functioning monitoring system will enhance our ability to predict failure, and will also increase the opportunity for early detection of problems that require addressing. Martin determined that an array system could function as a nervous system that could be used for crack and delamination detection, dynamic strain measurement, impact detection, and localization of damage on large structures.

Giurgiutiu et. al. (2002) also studied the use of piezoelectric sensors as an embedded structural health monitoring technique. In their study the behaviour of piezoelectric active sensors were used to detect near field and far field damage in aircrafts. Piezoelectric sensors were chosen due to their small, noninvasive nature, and because they are inexpensive and easily wired into arrays. Giurgiutiu (2002) determined that unobtrusive piezoelectric sensors can successfully monitor the structural health of aircraft structures. A distinct advantage of this type of system over a strain gage system is that a piezoelectric sensor can provide information about the test specimen performance at both near and far distances from the sensor (Giuriutiu 2002). Additionally, piezoelectric materials can withstand large strains without severe distortion (Wei Chih et. al 2002). A disadvantage of the piezoelectric sensor is that they require electrical conducting copper wires to operate, and they are more intrusive than other systems such as the active fibre waveguide sensors, (Atkinson and Hayward 2001) and the material is easily damaged mechanically (Wei Chih et. al. 2002).

2.9.2.2 Resonance Similarly, vibrations and frequencies within a structure have been used for non-destructive analysis. Since all structures resonate with a natural frequency (Adams and Cawley 1979), it is possible to observe and measure changes in this frequency to pin point localized damage, whether that be a crack or a change in material stiffness. This method will uncover any damage that has occurred, but will provide limited details regarding the severity of damage (Adams and Cawley 1979).

2.9.2.3 Active Fibres Benefits of active fibre waveguides include their ability to withstand high temperatures and pressures associated with composite manufacturing (Atkinson and Hayward 2001). Embedding active fibres into a structure provides a means to introduce ultrasound to the structure which generates waves, whose behaviour can be analyzed to determine structural performance (Atkinson and Hayward 2001). Optical fiber sensor arrays have also been used to create an array that measures the pressure and stress distribution in human feet, as shear stress in the lower extremities has been found to be a contributing factor to foot ulcers in diabetics (Wei-Chih et. al. 2002).

2.9.2.4 Acoustic Methods Acoustic methods have been used for structural health monitoring of concrete filled steel pipes that are used for supporting civil and marine structures (Kundu and Na 2002). The reflection, transmission, and scattering of acoustic waves provide information from which the structural health of the pile can be determined. Cylindrically guided acoustic waves (Lamb waves) are sensitive to pipe defects and mechanical damage to pipes (Kundu and Na 2002). Acoustic monitoring offers the

advantage that guided waves can propagate for long distances (Kundu and Na 2002) and therefore increase the flexibility in the testing apparatus. Additionally, the use of electro-magnetic acoustic transmitters to create the wave instead of using piezoelectric sensors allows for a physical separation between the test equipment and the test specimen, therefore reducing the effects of the test equipment on the test results (Kundu and Na 2002).

The bond integrity of small diameter polymeric medical tubing can also be determined using an acoustic method known as acousto-photonic nondestructive evaluation (TAP-NDE). In this scenario, a laser generates ultrasonic waves in the tubing, which are detected by a fiber-tip interferometer and HeNe laser. The study examined bond defects caused by tensile pull, needle puncture, and crease and determined that flaws in the generated dispersive waves were distinct for each different bond flaw (Harms and Suh 2002). Distinct flaws in the generated dispersive waves were also observed for stiffening effects in the plastic tubing. The research concluded that laser optic based ultrasonic techniques are appropriate for the non-destructive evaluation of small diameter tubing.

In another study, it was shown that the surface wave velocity distributions of sound and defective specimens showed significant differences (Miyasaka and Tittmann 2002). This means that scanning acoustic microscopy can be used to determine the integrity of ceramic to metal joints (Miyasaka and Tittmann 2002).

2.9.2.5 Photoelastic Methods Photoelastic theory states that the velocity of light through a body is dependent on the stress level in that body (Stanley 1977). Therefore, polariscope techniques can be used to determine principle stress values in materials that transmit light. Observations and quantification, or calibration, of this phenomenon make it easy to determine the stress levels of transparent specimens. Fessler and Woods (1982) were able to use photoelastic stress analysis techniques to determine the effects of shape and position of load application on the peak stress in flat bars. This allowed for a determination of stress concentrations for any practical bar shape. Photoelastic techniques have also been successfully used to measure stress levels in the welded joints of off-shore platforms (Fessler and Little 1981). Unfortunately, the principles of this technique dictate that it is most applicable to transparent or translucent materials, and therefore it is not a valuable stress analysis technique in most biological situations.

2.10 Structural Modelling

Structural modelling and analysis is valuable in many engineering disciplines, including aerospace engineering, biosystems engineering, civil engineering and mechanical engineering (Dym 1997). Various approaches toward developing structural models have been developed in the past including energy methods, rigorous mathematical and calculus derivations and systems theory (Dym 1997; Carmichael 1981). A common theme in the development of structural models is the simplification or reduction of a large system into smaller subsystems that lend themselves to structural analysis techniques. Structural modelling processes are well understood in the engineering field, and their continued development and progression will optimize structural design. Modelling can also be

characterized as constructing a mathematical model that represents the geometry and other parameters of the subject structure, and computing the displacements and stress resultants at every point in the structure (Elezaby and Simmonds 1992).

2.10.1 Basic Concepts of Structural Modelling

The six elements of structural design that contribute to the formation of a structural model are loads, reactions, internal forces, stresses, strains, and displacements and deflections (Dym 1997). These six fundamental elements are related to each other through equilibrium laws, constitutive laws and compatibility. Equilibrium laws refer to Newton's second law, constitutive laws are those that define the material from which a structure is made and their stress-strain relationship and compatibility refers to a consistency of physical properties and the compatibility of strains and deflections (Chen and Saleeb 1982).

Structural models based on the theory of elasticity are useful for describing the behaviour of structures at their working level (Chen and Saleeb 1982). These models are useful for isotropic and anisotropic materials and therefore are reasonable indicators of expected performance in wood framed buildings.

Mathematical programming is used to reduce the complexities of a system into its subsystems for which structural analysis can be performed. This often involves the conversion of non-linear problems into linear problems using the cutting plane method (Carmichael 1981).

2.10.2 Applications of Structural Modelling

Structural modelling has been used throughout the field of engineering including the design and analysis of vibrating structures (Beards 1983), the study of stability and ductility of steel structures under cyclic loading (Fukomoto and Lee 1992) and the study of structural dynamics (Kratzig et. al. 1991). This paper will not delve into the vast amounts of literature available regarding the performance of structural modelling techniques, as the purpose is to evaluate if structural modelling whether through step-by-step mathematical analysis or through the efficiencies granted by modern software can be relied upon to accurately represent the behaviour of structures of interest, including post-frame buildings.

2.11 Post-Frame Buildings

A particularly valuable application of non-destructive evaluation and strain measurement is the study of post-frame buildings. More advanced understanding of the properties and performance of post-frame buildings will allow for more efficient design, and earlier detection of possible structural deficiencies. A brief review of post-frame history, design, and use will help to understand the direction and purpose of current research.

2.11.1 History and Building Design

Post-frame buildings are economical and adaptable structures that are commonly found used in agricultural applications (Irish et al. 1976). Modern post-frame building design has evolved from the earlier pole-frame designs of the 1930's when H. Howard Doane

combined posts with metal roof sheeting to make the first post-frame building of the modern age (Walker and Woeste 1992). Pole-frame buildings originally became popular in a large part due to their ease of construction and low building cost. As time passed, the variable diameter poles were replaced with posts of constant dimensions, and other design details such as eliminating the use of knee braces furthered the development of the post-frame building (M.G. Britton, Associate Dean, University of Manitoba).

In a post-frame building, posts are used as the main structural elements that transmit roof loads down into the earth (Walker and Woeste 1992). The posts and roof must be capable of resisting all applied loads without undergoing undue deformation
(Manbeck et al. 1992). Post-frame buildings do not require any foundation aside from the interaction of the posts with the sub grade into which they are installed. Since the posts directly transfer roof loads into the earth, no concrete footings or piles are required. The roof design typically includes engineered truss systems similar to those found on other building types, and the walls can be constructed either with conventional building materials or alternative building materials such as straw bales.

2.11.2 Issues Facing Post-Frame Building Design

Calculations using accepted structural engineering design methods and structural modelling through commercial software packages produce results that indicate that post-frame buildings are not stable. This has created a situation where obtaining approval from regulatory or funding agencies for the construction of a post-frame building has become extremely difficult. Alternatively, designers of post-frame buildings believe that

they are stable, and point to the success of post-frame construction in North America as visible examples. It is obvious that a more detailed understanding of the structural properties and behaviour of post-frame buildings is required, and that new design methods and software are needed.

Early designs of post-frame buildings were based on the assumption that all loads were transferred to, and carried by, the post-frame bents. This method of analysis ignores the large contribution of diaphragm action toward the overall strength of a post-frame building. Bohnhoff et. al. (1990) define diaphragm action as the redistribution or transfer of loads by the building diaphragms, where the diaphragms are formed by the building cladding. Diaphragm analysis of a post-frame building shows that the majority of wind loads exerted on the side of the building are carried by the wall material, and that only a small portion of the overall load is exerted on the post (Walker and Woeste 1992). Additionally, wind loads applied horizontally at the building's eave are transferred horizontally by the roof and ceiling diaphragms to the end walls of the building, where they are transferred by the posts into the ground (Bonhoff 1992). This allows for a less conservative post design, which in turn leads toward a more economical building. For example, in a 10 m wide by 20 m long post-frame building, considering the diaphragm action of metal cladding allows for a reduction in post design in the order of one nominal size.

It must be said, however, that this design method is only acceptable in one storey buildings with end walls sufficiently rigid to transfer shear loads from the roof to the

ground. The large discrepancy in overall building design that results from the two different design methods mentioned, usually leads to some discomfort from regulatory agencies in accepting designs based on diaphragm analysis. This is because diaphragm analysis is not routinely use in the analysis of normal commercial buildings, since the contribution of diaphragm action to the overall strength of non light-framed buildings is negligible.

Non-destructive evaluation will provide the more detailed understanding of post-frame building properties and performance that is required to optimize their design, and ensure their safe operation.

2.12. Conclusion

The stress-strain relationship that exists for all materials provides for a convenient, relatively easy method of behaviour analysis, namely strain measurement with strain gages. As strain gage technology continues to improve, more accurate and precise results will be produced, and fewer sources of error will have to be considered. The versatility of the modern strain gage has provided an incredible opportunity for researchers, engineers, and scientists to study and understand the physical properties of elastic materials, and it holds to reason that further advances in the field of strain measurement will allow us to expand our knowledge of the behaviour of non homogenous materials such as wood and composite materials. Information gathered from strain measurement will also continue to be a valuable resource in the validation of new stress analysis and

non-destructive evaluation techniques, which in turn enables optimization of building design and ensures safe operation of structures.

3.0 OBJECTIVES

Through a review of the stress and strain relationship in physical materials and their application to the field of non-destructive evaluation, this thesis aims to develop a method of strain measurement appropriate for dimensional lumber used for the structural members of a light-frame building. Based on information gathered in the literature review, a method of calibrating a wood strain gage at a lab scale will be examined. Ideally, this method of strain measurement will allow a comparison of the actual performance of a post-frame building to the results of predictive calculations and the results of a structural model created using RISA-3D, a structural modelling software program.

The research portion of this project examines the effectiveness of different materials, their dimensions, and the assembly procedures used in the development of a calibrated wood strain gage. A structural model will be developed following this lab-based structural research to allow for comparison of expected and achieved results.

Particular objectives are:

1. Determine the feasibility of developing a wood strain gage that will provide accurate, precise, and reliable information regarding the stress of structural members in light-framed buildings.
2. Examine the use of wood materials and their strain response to an induced stress.
3. Examine the use of acrylic materials and their strain response to an induced stress.

4. Measure the stress-strain relationships for strain gages mounted on test specimens, and measure the stress-strain relationships for that test specimen when mounted on dimensional lumber.
5. Compare the stress-strain relationships for the two phases and determine if a consistent correlation exists.
6. Develop a structural model of a post-frame building at the University of Manitoba
7. Compare the results of the structural model to results expected based on the measured properties of the lab tested specimens.

4.0 THE DEVELOPMENT OF A CALIBRATED WOOD STRAIN GAGE

4.1 Introduction

Structural analysis of biological materials such as wood is an uncertain science based on formulas developed for homogenous, isotropic materials. Since wood is heterogeneous and anisotropic there are additional uncertainties to consider when analyzing its performance, and due diligence requires that the designer err on the side of caution. The result of this is a potential for an over conservative approach and lost efficiency in the design and construction of light-framed buildings.

Modern structural design is based on an understanding of the physical properties of building materials and their performance when subjected to structural loads. For certain types of building material, like steel, these properties are thoroughly understood and the relationship between strain and stress is clearly defined. In other building materials, like wood, these relationships are based on a wider distribution of measured values, and therefore engineering designers are forced to deal with more uncertainties in structural design. The heterogeneous nature of wood requires that various factors be considered during structural design including service factor, size factor, and treatment factor. In addition, the anisotropic nature of wood requires that the appropriate design value be selected according to the proposed end use of the wood materials.

Non-destructive analysis techniques can be applied to light-framed buildings in order to determine if their actual performance is consistent with the expected performance as

determined by structural analysis. While these non-destructive evaluation techniques are well developed and applicable to materials with consistent physical properties such as steel, their usefulness is diminished when considering the performance of biological materials. Therefore, a research study based on strain measurement was initiated with the purpose of developing a technique useful for the non-destructive evaluation of light-framed buildings.

Strain measurement is a tool that has been used with great success in the 20th and 21st century for evaluating the physical effectiveness of structural materials. Using Hooke's Law, the stress of a member can easily be calculated from a measured strain within the elastic range of a material. In the case of a material such as steel where its homogenous nature leaves little doubt regarding its physical properties, this calculation can be relied upon to provide accurate stress levels. However, in a heterogeneous and anisotropic material such as wood, the variation in physical properties between specimens creates an uncertainty regarding its physical properties, and therefore there is less confidence in the stress values calculated based on measured strains. The primary objective of this study is to develop a system that minimizes this uncertainty to a practical level.

Accurate strain measurement depends on the successful mounting of a strain gage to a test specimen. The detail necessary for the strain mounting procedure requires operator experience and the clean conditions of a laboratory. In the field, maintaining chemically clean surfaces and precisely following the step by step procedures of strain mounting is difficult and there are many opportunities to introduce error sources into the strain

measurement. A system where the first step involves the delicate procedures of strain gage mounting in a lab setting, and where the second step is to take the strain materials developed in the lab to the field for strain measurement, has the potential to decrease the possible error sources and increase the reliability of field strain measurement.

The procedure evaluated in this research program is to apply a strain gage onto a small specimen of wood or acrylic and determine that specimen's stress and strain relationship. This specimen would then be attached to a piece of dimensional lumber and the stress-strain relationship would once again be measured. A consistent relationship between the stress-strain curves would provide the calibration coefficient necessary to apply the technology to field measurement.

An important step in achieving the research goals is to develop the experimental methods and equipment necessary to perform the lab calibration. The construction of a research plan and the fabrication of appropriate testing equipment are the base requirements for the successful outcome of this research program. Developing a reliable experimental method presented challenges that resulted in ongoing modifications to materials and methodology. Experimental techniques were improved over the course of the experiment in an attempt to reduce the variables affecting the research and increase the accuracy and precision of the testing. As a result, a major portion of research efforts were directed towards developing equipment and selecting specimen dimensions that allowed for consistency in loading procedures in the ATS test frame.

4.2 Materials and Methods

4.2.1 Site Description

Experimental stress and strain analysis was completed in the Physical Properties Lab in the Biosystems Engineering Building at the University of Manitoba in Winnipeg, Manitoba.

4.2.2 Equipment and Supplies

The equipment used in the Physical Properties lab experiments included a P – 3500 Strain Indicator from Measurements Group – Instruments Division of Raleigh, North Dakota; a No. 3052-01 0.01 – 30 mm Dial Indicator from Mitutoyo; a Series 1410 10000 pound computer controlled universal testing machine from Applied Test Systems Inc. in Butler, Pennsylvania; 350 Ω metal foil resistance strain gages from Vishay Micro-Measurements; terminal strips; AE-10 adhesive from Vishay Micro-Measurements, 5 Minute® Epoxy Gel from Devcon, 400grit sandpaper, spring clamps, strain gage tape, pink pearl erasers, personal computer, pine wood, #2 SPF 38 x 89 mm dimensional lumber, drill press, lathe, steel cylinders, mitre saw, table saw, and acrylic. Figure 4.1 shows the ATS testing apparatus and some of the various equipment used in the research.

Fig. 4.1. Test apparatus including ATS machine and computer controls.

4.2.3 Experimental Design

The successful completion of the research program required developing a test method, identifying and obtaining the required equipment, fabricating required tools, and carrying out the testing.

The first step of the experimental program was to develop a test method that produced consistent stress-strain curves for each gage in the calibration phase. The calibration phase of this program required mounting the gage onto a test specimen and subjecting the

specimen to a known force and recording the strain measurement at the surface of the specimen. The structural phase of the program consisted of mounting the calibration gages on a 38 x 89 mm member and measuring the strain under controlled loading. The calibration and structural phase of each treatment consisted of a minimum of three loading cycles. The hypothesis was that a correlation should exist between the stress-strain curves developed from the calibration and structural phases. The Results and Discussion section will examine the varied levels of success that were experienced in this regard.

The procedure was to create a "wood strain gage" or "acrylic strain gage" by mounting a metal foil resistance strain gage onto a small piece of maple wood or acrylic. The strain gage mounting process for the wood strain gage followed the following step by step procedure as recommended by Vishay (Vishay Micro-Measurements 2005):

1. Prior to beginning the strain gage mounting procedure, the wood specimen was coated with a layer of adhesive and allow to cure.
2. Once the adhesive cured, all of the adhesive external to the wood specimen was removed by sanding the adhesive until the surface of the wood specimen was exposed. This step was necessary so that pores at the surface of the wood specimen became saturated with adhesive and therefore would not soak in any adhesive at the time of strain gage mounting.
3. The surface of the wood specimen was cleaned using water and degreased using isopropyl alcohol.

4. Gage layout lines were etched into the wood specimen to assist in positioning the gage at the time of gage mounting.
5. The wood specimen was cleaned again using water and degreased again using isopropyl alcohol.
6. The gage and terminal strips were positioned on the wood specimen in accordance with the grid layout lines.
7. Using strain gage tape, the gage was picked up off of the wood specimen exposing the underside of the gage as shown in Figure 2.2.
8. The resin and the hardener of the two part epoxy were combined and mixed for the recommended five minute period.
9. A thin layer of epoxy was applied to the surface of the wood specimen and the underside of the gage, as shown in Figure 2.3.
10. The gage was repositioned onto the wood specimen and clamped using spring clamps and Pink Pearl erasers to evenly distribute the clamping force.
11. The epoxy was allowed to cure for a minimum of 24 hours.
12. Wires were soldered from the terminal ends of the strain gage to the terminal strips.
13. The lead wires were soldered to the terminal strips.

Figure 4.2 depicts a strain gage mounted onto one of the wood specimens tested in Treatment A.

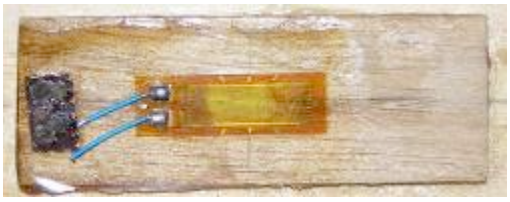

Fig. 4.2. A metal foil resistance strain gage mounted onto a wood calibration specimen.

In the case where acrylic specimens were used rather than wood the same procedure was used with the exceptions of replacing steps one to five with the following:

1. The acrylic specimen was cleaned with water and degreased using isopropyl alcohol.
2. The surface of the acrylic specimen was conditioned using Conditioner A.
3. The surface of the acrylic specimen was neutralized using Neutralizer.
4. Gage layout lines were etched into the acrylic specimen to assist in positioning the gage at the time of gage mounting.

The wood or acrylic specimen on which the strain gage was mounted was then subjected to a longitudinal compression force of known magnitude using the ATS test machine and the resultant strain was measured with a strain indicator. The load was limited to that which produced a strain reading of ~2000 micro strains, well within the 3000 micro strain limit of the strain gages. Figure 4.3 shows the strain indicator that was used. Calculations of the factored compressive resistance and factored compression load were completed for each treatment.

Fig. 4.3. The strain indicator

With the known force and dimensions of the test specimen, the stress in the specimen was calculated using Equation 4.1., where it was assumed that the stress measured was the normal stress that was distributed over the surface of the wood specimen at the location of the gage.

$$\sigma = P/A \qquad \textbf{Equation 4.1}$$

A plot of stress-strain was created for the newly developed wood or acrylic strain gage.

In order to ensure consistency in the strain measurements, a loading mechanism that minimized the potential for induced error caused by off axis loading of the wood strain gage was developed. Creating slotted contact cylinders for the ATS machine as detailed in Figure 4.4, ensured that subsequent loading cycles of the wood strain gauge were completed in a consistent manner.

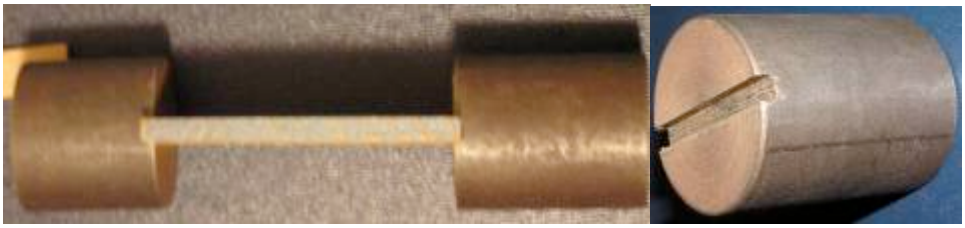

Fig. 4.4. Grooved loading cylinders used to ensure consistent loading procedures

Once the calibration phase of the wood or acrylic strain gages was complete, the gages were mounted onto 1.0 metre lengths of #2 SPF 38 x 89 mm dimensional lumber. A pretreatment of the 38 x 89 lumber was completed similar to that outlined in steps one & two of the wood strain gage preparation procedure. Once this pretreatment was complete, the wood or acrylic strain gages were mounted onto the 38 x 89 mm wood specimen using 5 Minute® Epoxy Gel and clamped using c-clamps with Pink Pearl erasers to distribute the clamping force. The gages were given a minimum of 24 hours to cure. Figure 4.5 shows one of the test members with various calibration gages mounted on its surface.

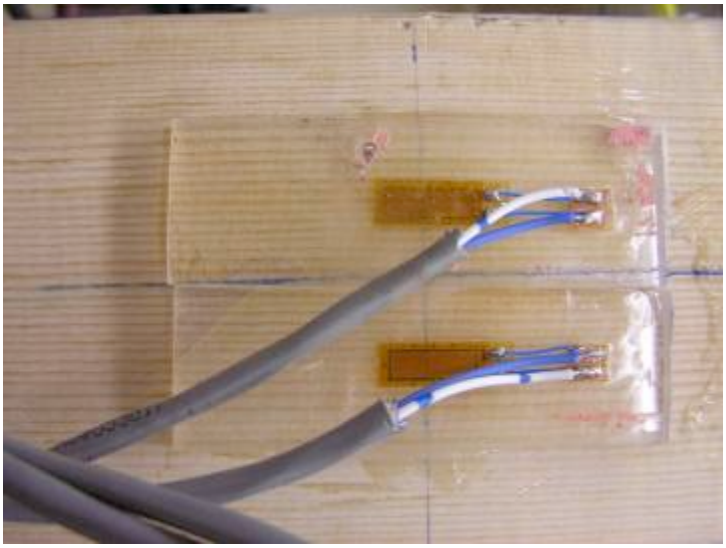

Fig. 4.5. Calibrated acrylic gages mounted onto the 38 x 89 mm member.

The 38 x 89 mm test specimens were subsequently subjected to loading cycles similar to that of the acrylic and wood strain gage calibration tests. Recessed cylindrical notches as shown in Figure 4.6 were created at each end of the 38 x 89 mm member to ensure that the load was applied in the same manner for each repeated experiment. Figure 4.7 shows the load being applied through a cylinder in the recessed end of the 38 x 89 mm member.

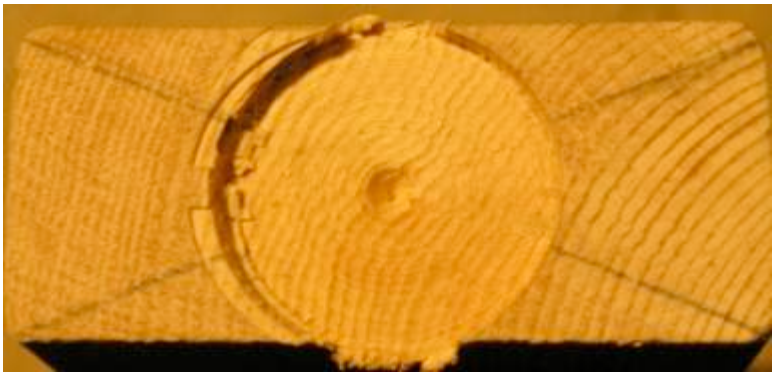

Fig. 4.6. The cylindrical recess on the end of the 38 x 89 mm member that allowed for consistent loading of the assembly.

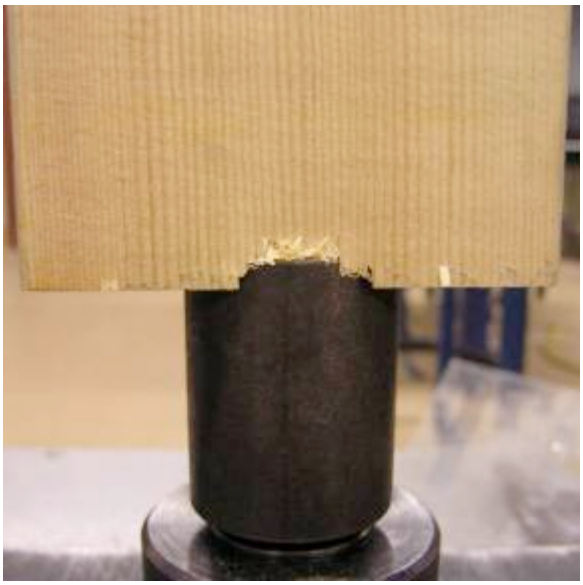

Fig. 4.7. The loading cylinder and the 38 x 89 member under test conditions.

The gage calibration phase and gage testing phase were completed for wood specimens with dimensions of 5 x 13 x 40 mm, 5 x 40 x 100 mm, and 2 x 20 x 50 mm, and for acrylic specimens with dimensions of 3 x 25 x 75 mm. Figure 4.8 shows the four different calibration specimens tested and gives an idea of their relative sizes (a penny is provided for scale). The size and dimensions of the wood and acrylic specimens were selected to minimize any influence on the strain performance of the metal foil resistance strain gage, and to minimize any stiffening effects on the 38 x 89 mm specimen.

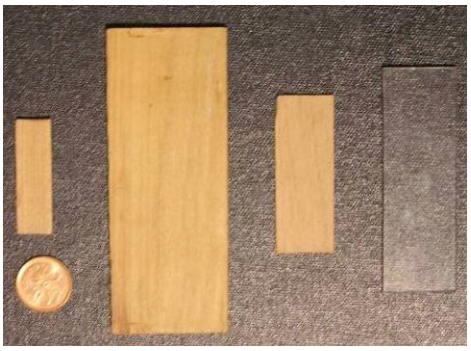

Fig. 4.8. The four different calibration specimens and a penny for size reference.

Upon completion of experimental testing, the stress-strain curves for the calibration and structural phases were compared.

Statistical analysis was completed for each treatment to determine if a correlation between the two curves was consistently produced within an acceptable range. In the case where a clear correlation could be determined, the calibrated gage would be suitable for use in non-destructive evaluation of other structures constructed of materials with the same properties as the 38 x 89 mm wood specimen.

4.3 Results and Discussion

4.3.1 General Calculations

The calculation represented in Equation 4.2 indicated that a force of 10000 N would produce a normal stress of approximately 3 MPa in the 38 x 89 mm wood specimen, which was similar to the stress levels produced in the calibration testing of the acrylic and wood specimens for Treatments B, C, and D.

$$\sigma = P/A = 10000\ N/(38\,mm \bullet 89\ mm) = 2.96\ N/mm^2 = 2.96\ MPa$$

Equation 4.2

$$\sigma = 2.96\ MPa$$

The moment of inertia calculations represented by Equations 4.3 and 4.4 indicate that the wood and acrylic specimens had negligible stiffening effects on the 38 x 89 mm member, and therefore their influence on the bending capacity of the 38 x 89 mm member was ignored.

I of 38 x 89 alone

$$I = bd^3/12 = 89*38^3/12 = 406967$$

Equation 4.3

$$I = 406967$$

I of 38 x 89 mm member with largest calibration gage

$$I = b_1d_1^3/12 + b_2d_2^3/12 = 13*5^3/12 + 89*38^3/12 = 406967 + 135 = 407102$$

Equation 4.4

$$I = 407102$$

$$Difference = 407102 - 406967 = 135 \; and \; {}^{135}\!/_{406967} = 0.03\% \Rightarrow negligible$$

Equations 4.5 to 4.11 calculate the factored load and factored compression and bending resistance of the 38 x 89 mm specimen. As shown, the compressive resistance is less than the factored compression load, and therefore an applied load of 10 kN is acceptable.

Certain design assumptions were made in order to facilitate the following calculations. All assumptions were based on the information contained in CSA 086.1-01. The specified bending strength, f_b, was taken as 11.5 MPa in accordance with Table 5.3.1A of O86-01 (CSA). The load duration factor, K_D, was taken as 1.15 since the duration of the loading during the experiment was less than 7 days. The system factor, K_H was taken as 1 since the wood and acrylic specimens were being subjected to compressive loads but were not a part of a system of 3 or more members spaced not more than 610 mm apart. The service condition factor for compression K_{sc}, was determined to be 1.0, the factor for dry service conditions. The treatment factor K_T, was also taken as 1.0 since the subject wood specimens were untreated. All other values and factors were determined in accordance with the applicable formulas and calculations.

$$Factored\ Compression\ Force = P_f$$

$$P_f = \alpha_L \times L = 1.5 \times 10\ kN = 15\ kN \qquad \textbf{Equation 4.5}$$

$$P_f = 15\ kN$$

$$Factored\ Compression\ Load\ Resistance\ Parallel\ to\ the\ Grain = P_r$$

$P_r = \phi F_c A K_{zc} K_c$; **where** **Equation 4.6**

$\phi = 0.8$

$F_c = f_c(K_D K_H K_{sc} K_T) = 11.5(1.15 \times 1 \times 1 \times 1) = 13.2\ MPa$ **Equation 4.7**

$A = cross\ sectional\ area\ = 38 \times 89mm = 3382mm^2$

$K_{zc} = 6.3(dL)^{-0.13} = 6.3(89 \times 1000)^{-0.13} = 1.43\ by\ rule\ use\ 1.3$ **Equation 4.8**

$$K_C = \left[1.0 + \frac{F_C K_{zc} C_c^{\,3}}{35 E_{05} K_{SE} K_T}\right]^{-1} = \left[1.0 + \frac{13.2 \times 1.3 \times 26.3^3}{35 \times 5000 \times 1 \times 1}\right]^{-1} = 0.36$$ **Equation 4.9**

$C_c = {}^{L_e}\!/_{b}\ or\ {}^{L_e}\!/_{d} = {}^{1000}\!/_{38} = 26.3\ or\ {}^{1000}\!/_{89} = 11.2\ choose\ larger$

Equation 4.10

$C_c = 26.3 < 50 \therefore OK$

$L_e = K_e L = 1.0 \times 1.0 = 1.0$ **Equation 4.11**

$P_r = \phi F_c A K_{zc} K_c = 0.8 \times 13.2 \times 3382 \times 1.3 \times 0.36 = 16.7\ kN$

$P_r = 16.7\ kN$

Since $P_r = 16.7\ kN$ *and* $P_f = 15\ kN$, *then* $P_f > P_r$ *and therefore design is ok for axial compression load*

4.3.2 Treatment A

4.3.2.1 Part 1 Treatment A was the original experiment and consisted of mounting four gages on four wood specimens with approximate dimensions of 40 x 13 x 5 mm. Table 4.1 lists the actual dimensions of each individual specimen.

Table 4.1. Dimensions of the specimens tested in part 1 of Treatment A

Gage	Length (mm)	Width (mm)	Depth (mm)
A1	39.1	11.6	4.7
A2	39.4	11.4	4.5
A3	40.2	13.5	5.0
A4	38.9	13.0	4.8

The wood specimens were subjected to compression forces parallel to the wood grain. Table 4.2 indicates the maximum force that each wood specimen was subjected to, and the calculated compressive resistance of each specimen as determined through equations 4.12 to 4.19, which represent the calculations for the design dimensions of 40 x 13 x 5 mm. Gage A1 was accidentally damaged during experimentation and is not included in the remainder of the results for Treatment A.

Table 4.2. The factored compressive capacity of Treatment A specimens (part one) and the factored compressive load applied.

Gage	Compressive Capacity (kN)	Factored Maximum Axial Compression Force // to Grain (kN)
A2	0.8	2.3
A3	0.8	1.8
A4	0.8	1.4

Factored Compression Force = P_f

$P_f = \alpha_L \times L = 1.5 \times 1.5\ kN = 2.3\ kN$ **Equation 4.12**

$P_f = 2.3\ kN$

Factored Compression Load Resistance Parallel to the Grain = P_r

$P_r = \phi F_c A K_{zc} K_c$ **; where** **Equation 4.13**

$\phi = 0.8$

$$F_c = f_c(K_D K_H K_{sc} K_T) = 11.5(1.15 \times 1 \times 1 \times 1) = 13.2\ MPa$$ **Equation 4.14**

$$A = cross\ \text{section}al\ area\ = 5 \times 13mm = 65\ mm^2$$ **Equation 4.15**

$$K_{zc} = 6.3(dL)^{-0.13} = 6.3(13 \times 40)^{-0.13} = 2.8\ by\ rule\ use\ 1.3$$ **Equation 4.16**

$$K_C = \left[1.0 + \frac{F_C K_{zc} C_c^{\ 3}}{35 E_{05} K_{SE} K_T}\right]^{-1} = \left[1.0 + \frac{13.2 \times 1.3 \times 8.0^3}{35 \times 5000 \times 1 \times 1}\right]^{-1} = 0.95$$ **Equation 4.17**

$$C_c = {}^{L_e}\!/_{b}\ or\ {}^{L_e}\!/_{d} = {}^{40}\!/_{5} = 8.0\ or\ {}^{40}\!/_{13} = 3.1\ choose\ larger$$ **Equation 4.18**

$$C_c = 8.0 < 50 \therefore OK$$

$$L_e = K_e L = 1.0 \times 0.040 = .040$$ **Equation 4.19**

$$P_r = \phi F_c A K_{zc} K_c = 0.8 \times 13.2 \times 65 \times 1.3 \times 0.95 = 0.8\ kN$$

$$P_r = 0.8\ kN$$

As shown, the applied axial compression force exceeded the 5th percentile design compressive capacities as calculated in accordance with CSA O86-01. However, physical damage was not observed on any of the wood specimens and at this stage and it was determined that continued testing was warranted.

The stress-strain curves developed from the calibration of Gages A2, A3, & A4 are represented in Figure 4.9. This graph indicates the stresses and strains recorded during a minimum of three loading cycles. Table 4.3 indicates the equation of the best-fit linear regression trend line and the associated R^2 value.

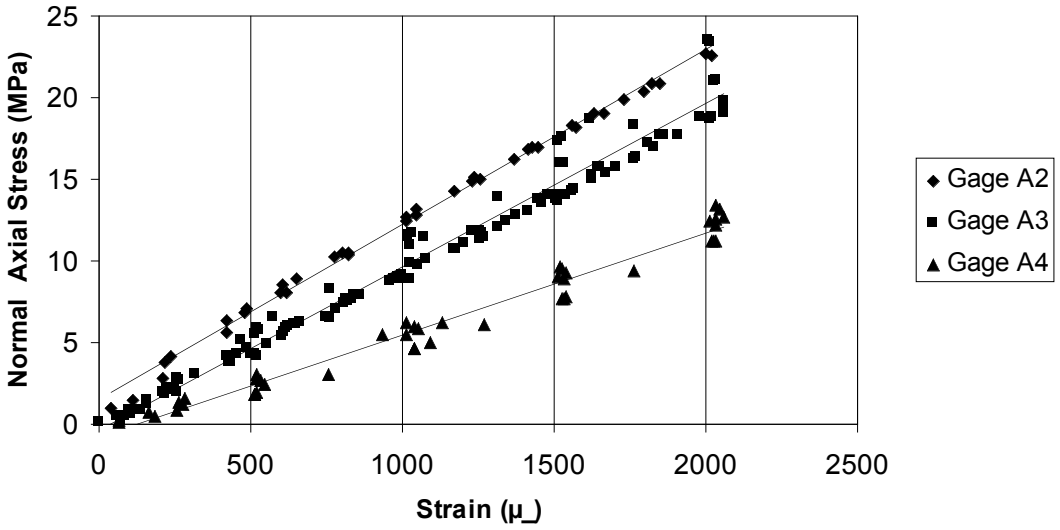

Fig. 4.9. The stress-strain curves for calibration phase of part one of Treatment A

Table 4.3. The stress-strain curves and regression coefficients for the calibration phase of part one of Treatment A.

Gage	Equation of Curve	R^2 Value
A2	y = 0.0107x + 1.4652	0.9957
A3	y = 0.01x - 0.3218	0.9731
A4	y = 0.0062x - 0.7188	0.9717

The results of this phase of Treatment A indicated that the calibrated wood strain gages performed as expected, with a generally linear relationship between the applied stress and resultant measured strain. During experimentation, Gage A2 was over stressed and determined to be unsuitable for further testing.

After the successful calibration of Gages A3 and A4, they were bonded to a one metre length of 38 x 89 mm SPF No 1/2 dimensional lumber.

This specimen was then subjected to a minimum of three cycles of axial loading in the ATS test machine. Mid-height deflections of the 38 x 89 mm lumber were recorded using a dial indicator with an accuracy of 0.01 mm. A deflection curve was developed based on these observations and is shown in Figure 4.10. The bending stress at the surface of the 38 x 89 mm lumber at the location of the gage was calculated based on the best-fit linear regression curve from Figure 4.10 and the applied moment in accordance with Equation 4.20 with Figure 4.11 indicating the direction of flexure. The applied moment was determined from the compression force and the displacement as determined by the best-fit linear regression curve. The bending stress was then subtracted from the total observed stress to remove bending effects from the analysis.

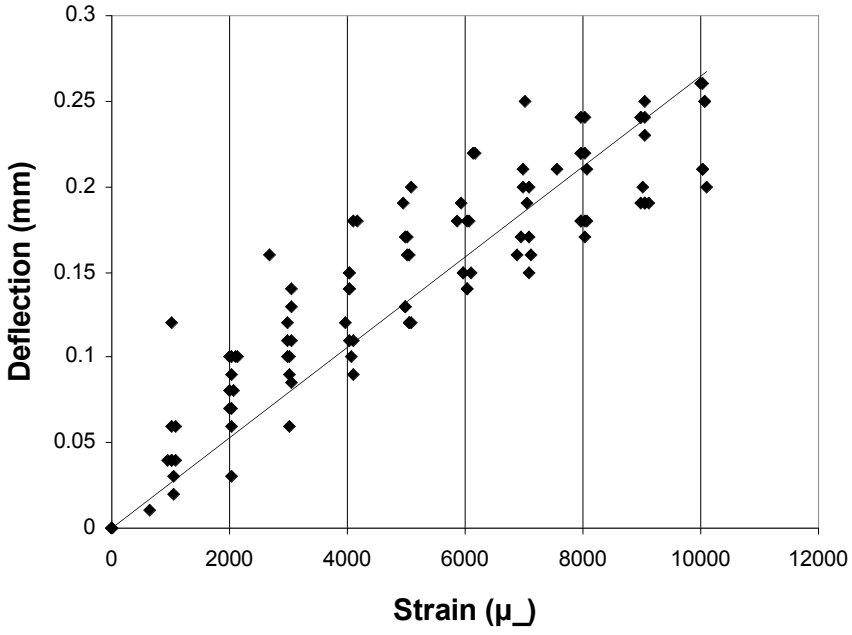

Fig. 4.10. The mid-height deflection of the 38 x 89 mm member under loading

$f_b = \frac{My}{I_{xx}}$; **where** **Equation 4.20**

f_b = *Bending Stress*

M = *Moment due to Compressive Force and Displacement*

y = Distance *From the Neutral Axis to the Surface*

I_{xx} = *Moment of Inertia* = $bd^3/12$;

where

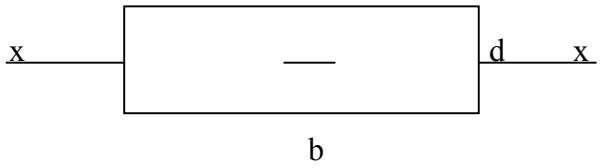

Fig. 4.11. The orientation of the 38 x 89 mm specimen on which the bending moment about the x-axis calculations was based.

Figure 4.12 indicates the stress-strain curves that were developed based on the results of this testing and Table 4.4 indicates the equation of the best-fit linear regression trend line and the associated R^2 value, as well as the ratio of the structural phase curve slope to the calibration phase curve slope. This ratio was determined by dividing the slope of the best-fit line of the calibration phase, by the slope of the best-fit line of the structural phase. If this ratio is consistent between specimens, then it will be possible to back calculate the force and stress of a structural member based on the strain reading of the calibrated wood specimen.

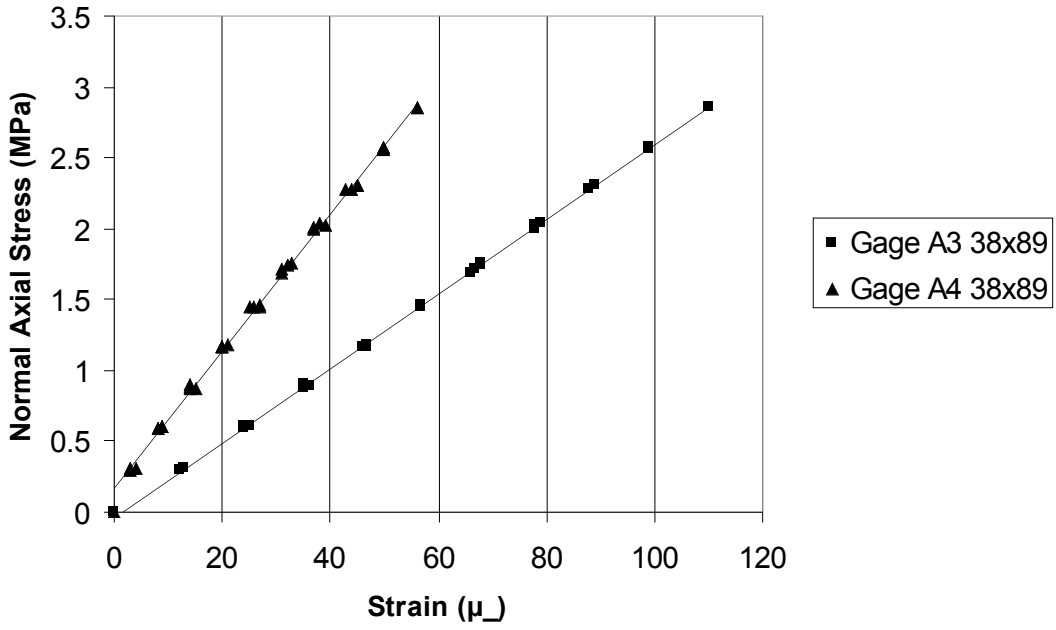

Fig. 4.12. The stress-strain curves for the structural phase of part one of Treatment A.

Table 4.4. The stress-strain curves and regression coefficients for the structural phase of part one of Treatment A, and the ratio between the slopes of the structural phase curve and the calibration phase curve.

Gage	Equation of Curve	R^2 Value	Slope Ratio
A3 on 38x89mm	y = 0.0262x - 0.0352	0.9998	0.38
A4 on 38x89mm	y = 0.0483x + 0.1726	0.9972	0.13

The results showed that there did not seem to be a consistent relationship or ratio between the curves of the best-fit linear regression lines of the calibration and structural phases. Therefore, it was inconclusive whether this experimental approach would provide the information required to satisfy the hypothesis. It was determined that the difference in strain measurement ranges between the calibration and structural phases was too large to offer proper comparison. As such, the calibration phase of the experiment was repeated

by applying only the forces that resulted in strains of similar magnitude to those measured in the structural phase. This testing constituted part 2 of Treatment A.

4.3.2.2 Part 2 In part 2 of Treatment A, two additional test specimens with dimensions shown in Table 4.5 were subjected to maximum strains of approximately 120 $\mu\varepsilon$ and maximum loads of approximately 120 N. This applied load was well under the 0.7 kN compressive capacity of the wood specimens as calculated and shown in Table 4.6. Gages A5 & A6 were calibrated following these restraints, and their stress-strain curves are presented in Figure 4.13. Table 4.7 indicates the equation of the best-fit linear regression trend line and the associated R^2 value.

Table 4.5. Dimensions of the specimens tested in part 2 of Treatment A

Gage	Length (mm)	Width (mm)	Depth (mm)
A5	39.6	12.7	4.8
A6	38.9	13.1	4.9

Table 4.6. The factored compressive capacity of Treatment A (part 2) specimens and the factored compressive load applied.

Gage	Compressive Capacity (kN)	Factored Maximum Axial Compression Force // to Grain (kN)
A5	0.8	.08
A6	0.8	.07

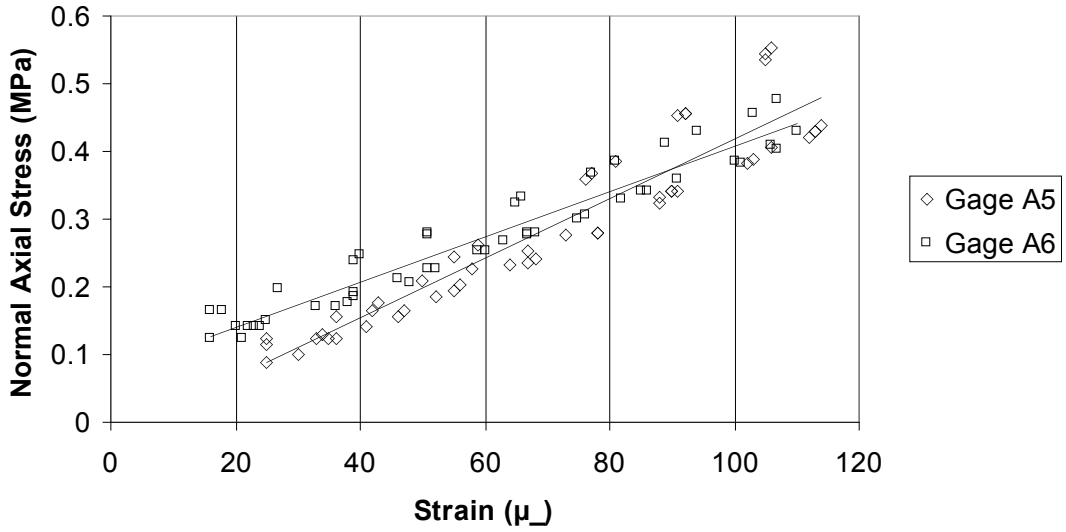

Fig. 4.13. The stress-strain curves for calibration phase of part two of Treatment A

Table 4.7. The stress-strain curves and regression coefficients for the calibration phase of part two of Treatment A.

Gage	Equation of Curve	R^2 Value
A5	y = 0.0044x - 0.0231	0.8894
A6	y = 0.0033x + 0.0743	0.9303

At the low loading levels experienced in this phase of the experiment, the reproducibility of the measured data was reduced. As a result the R^2 values are considered too low to allow for continued use of the experimental results as a base point on which to build towards the ultimate goal of developing wood strain gages.

The most likely error source contributing to the poor linearity of the stress-strain curves at low stress levels was the difficulty in manipulating the small wood specimen size into exact positions in the test apparatus. A slightly different configuration of the test specimen from one treatment to another may result in a large variation in measured strain

results for a given load. This was likely due to the influence of off centre loading and the introduction of bending stress. It was determined that a modified testing apparatus and a larger specimen size would be more favourable for the gage calibration process as it would allow for exact replication of experimental conditions between treatments. The calibration of the larger specimen sizes is discussed in the following section.

4.3.3 Treatment B

Treatment B consisted of mounting four metal foil resistance gages on wood specimens with dimensions of approximately 5 x 40 x 100 mm. Table 4.8 lists the actual dimensions of each individual specimen. As in Treatment A, the dimensions of the wood specimen were selected based on their similar aspect ratio to the metal foil gage. The larger specimen size compared to those used in Treatment A also allowed for more consistent positioning of the specimen in the strain measurement apparatus, and therefore increased the accuracy and precision of the calibration process.

Calibration of the wood strain gages was completed using the same procedures as in Treatment A. Figure 4.14 indicates the stress-strain curves for the four different wood strain gages. Table 4.10 indicates the equation of the best-fit linear regression trend line and the associated R^2 value.

Table 4.8. Dimensions of the specimens tested in Treatment B

Gage	Length (mm)	Width (mm)	Thickness (mm)
B1	99.1	39.5	5.0
B2	100.0	39.0	4.5
B3	102.7	39.4	5.0
B4	103.3	38.1	5.3

The wood specimens were subjected to compression forces parallel to the wood grain. Table 4.9 indicates that the maximum force that each wood specimen was subjected to was less than the calculated fifth percentile compressive resistance of each specimen.

Table 4.9. The factored compressive capacity of Treatment B specimens and the factored compressive load applied.

Gage	Compressive Capacity	Factored Maximum Axial Compression Force // to Grain (kN)
B1	1.4	0.9
B2	1.4	0.9
B3	1.4	1.1
B4	1.4	1.1

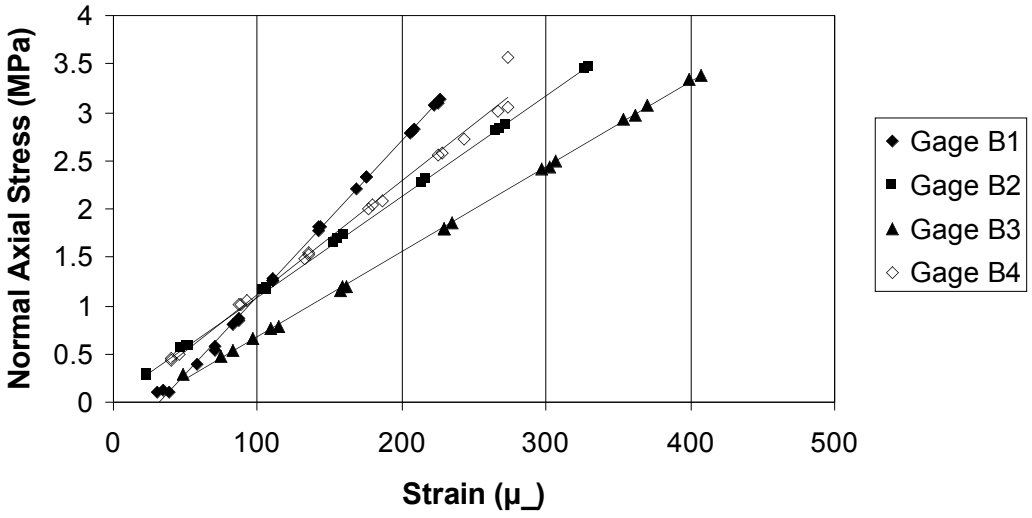

Fig. 4.14. The stress-strain curves for calibration phase of Treatment B

Table 4.10. The stress-strain curves and regression coefficients for the calibration phase of Treatment B.

Gage	Equation of Curve	R^2 Value
B1	y = 0.016x - 0.4983	0.9984
B2	y = 0.0104x + 0.0467	0.9998
B3	y = 0.0088x - 0.1941	0.9996
B4	y = 0.0118x - 0.0496	0.9872

It appeared as though all four gages performed well in the calibration phase of Treatment B, and were therefore mounted onto a one metre long specimen of 38 x 89 mm dimensional lumber for further testing. The resultant stress-strain curves are shown in Figure 4.15, and the equations of the best-fit linear regression analysis and the associated R^2 values, as well as the ratio of the structural phase curve slope to the calibration phase curve slope are shown in Table 4.11.

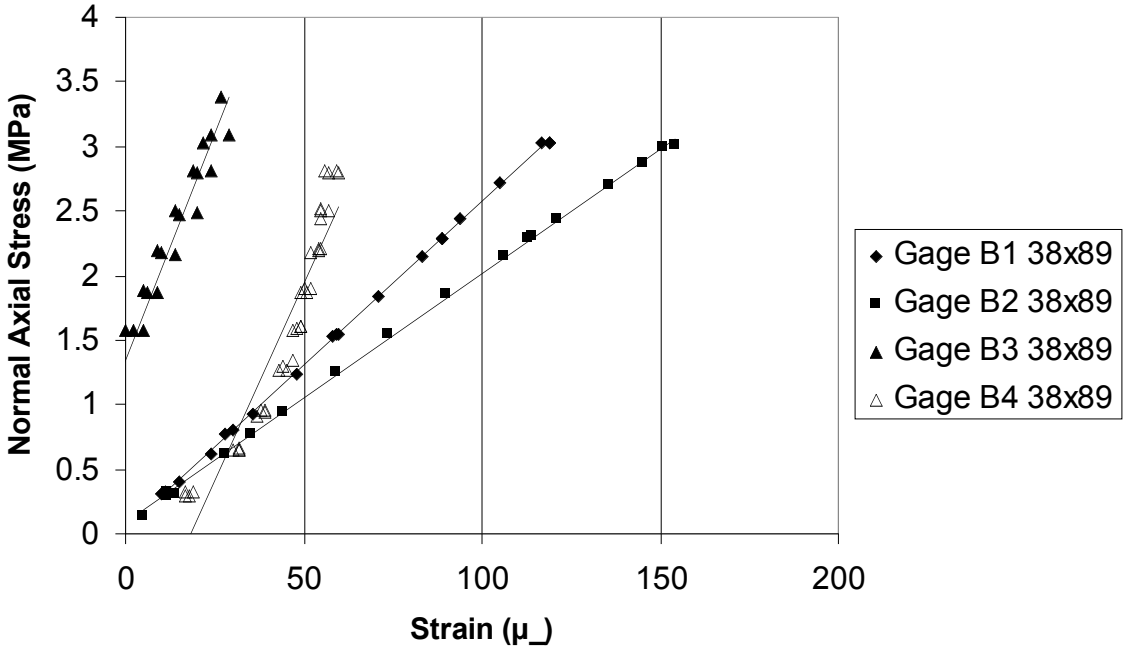

Fig. 4.15. The stress-strain curves for structural phase of Treatment B

Table 4.11. The stress-strain curves and regression coefficients for the structural phase of Treatment B, and the ratio between the slopes of the structural phase curve and the calibration phase curve.

Gage	Equation of Curve	R^2 Value	Slope Ratio
B1 on 38x89mm	y = 0.0253x + 0.0382	0.9997	0.63
B2 on 38x89mm	y = 0.0193x + 0.0856	0.9994	0.53
B3 on 38x89mm	y = 0.0708x + 1.3338	0.9212	8.95
B4 on 38x89mm	y = 0.0613x - 1.1393	0.8849	5.19

Gages B1 and B2 produced the expected linear curves and displayed strong R^2 values. However, the ratios of their slopes to the calibration curves were still not consistent enough to provide a comfort level that the gages could be used for accurate stress measurement of structural specimens. The relationship was however, stronger than that which was produced in Treatment A, and therefore there was promise to continue with further development and refinement of the experimental method.

Conversely, Gages B3 and B4 produced unexpected results that could not be used for data analysis. The logarithmic shape of the stress-strain curve for Gage B4 indicates that the gage was likely damaged during mounting and/or testing procedures. Similarly, the results for Gage B3 were likely excessively affected by induced bending stresses that are indicated by the movement of strains from the negative to positive sign.

Another suspected error source was the difference in physical properties that are inevitable in wood specimens the size of that tested. This is due to the heterogeneous nature of wood materials. Therefore Treatment C was designed using wood specimens half the size of those used in Treatment B in an attempt to reduce these heterogeneous effects and to reduce the thickness of the specimen that the stresses and strains would have to travel through to reach the metal foil strain gage. The intention was to minimize any strain losses that could occur due to creep effects and localized absorption or cushioning effects that could occur inside the cross sectional area of the wood specimen.

4.3.4 Treatment C

The calibration phase of Treatment C consisted of mounting four gages on wood specimens with dimensions of approximately 2 x 20 x 50 mm. Table 4.12 lists the actual dimensions of each individual specimen. Figure 4.16 indicates the stress-strain curves that resulted from the calibration phase of the strain gages, and Table 4.14 indicates the equation of the best-fit linear regression trend line and the associated R^2 value.

Table 4.12. Dimensions of the specimens tested in Treatment C

Gage	Length (mm)	Width (mm)	Thickness (mm)
C1	51.3	19.5	1.8
C2	51.2	18.3	1.8
C3	50.3	19.6	2.1
C4	51.6	19.3	1.7

The wood specimens were subjected to compression forces parallel to the wood grain. Table 4.13 indicates that the maximum force that each wood specimen was subjected to was less than the calculated compressive resistance of each specimen.

Table 4.13. The factored compressive capacity of Treatment C specimens and the factored compressive load.

Gage	Compressive Capacity (kN)	Factored Maximum Axial Compression Force // to Grain (kN)
C1	1.0	0.5
C2	1.0	0.5
C3	1.0	0.3
C4	1.0	0.3

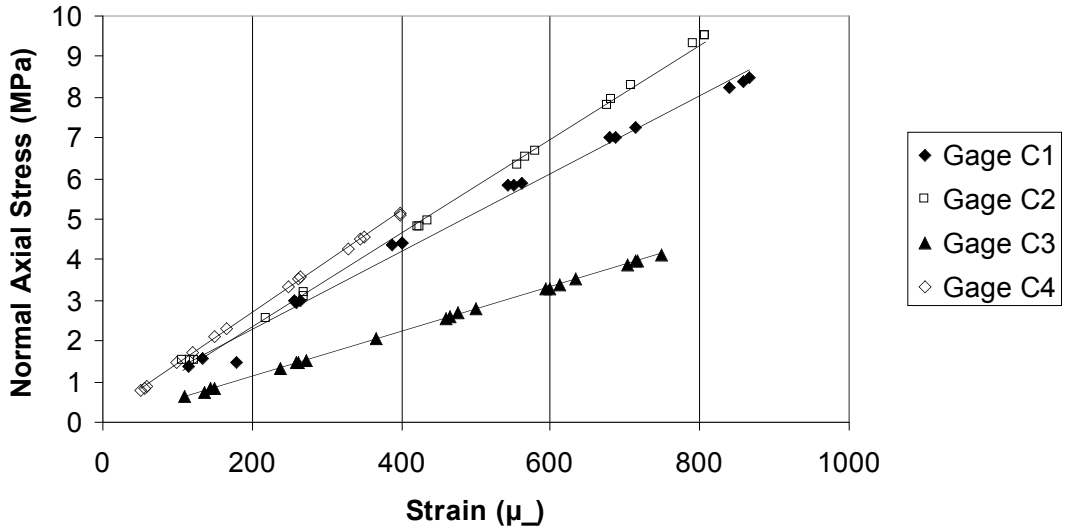

Fig. 4.16. The stress-strain curves for calibration phase of Treatment C

Table 4.14. The stress-strain curves and regression coefficients for the calibration phase of Treatment C.

Gage	Equation of Curve	R^2 Value
C1	y = 0.0096x + 0.3933	0.9921
C2	y = 0.0115x + 0.0482	0.9984
C3	y = 0.0055x + 0.0195	0.9998
C4	y = 0.0124x + 0.2099	0.9993

Each gage produced the expected linear stress-strain curve with strong R^2 values. Therefore, each calibrated wood gage was mounted onto a one metre piece of 38 x 89 mm dimensional lumber for the structural phase of Treatment C. Figure 4.17 indicates the stress-strain curves that resulted from those tests and Table 4.15 indicates the equation of the best-fit linear regression trend line and the associated R^2 value, as well as the ratio of the structural phase curve slope to the calibration phase curve slope.

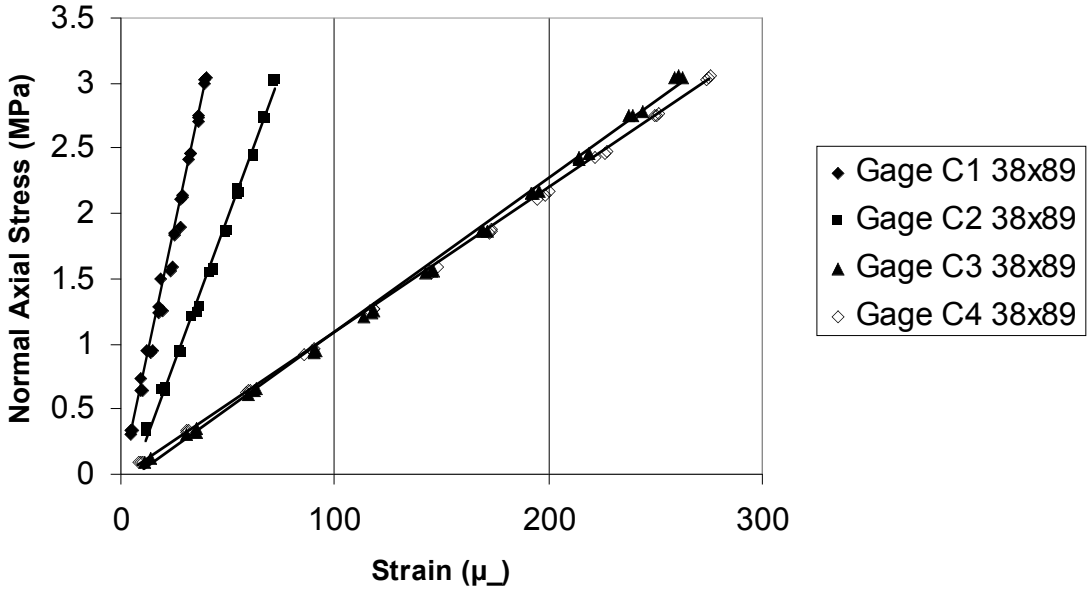

Fig. 4.17. The stress-strain curves for structural phase of Treatment C.

Table 4.15. The stress-strain curves and regression coefficients for the structural phase of Treatment C, and the ratio between the slopes of the structural phase curve and the calibration phase curve.

Gage	Equation of Curve	R^2 Value	Ratio of Slopes
C1 on 38x89mm	y = 0.0782x - 0.1181	0.9900	0.12
C2 on 38x89mm	y = 0.0444x - 0.2911	0.9951	0.26
C3 on 38x89mm	y = 0.0118x - 0.0992	0.9981	0.47
C4 on 38x89mm	y = 0.011x - 0.0264	0.9997	1.27

Figure 4.18 is a plot of the best-fit linear regression curves for the calibration and structural phase of the gage testing for Treatment C.

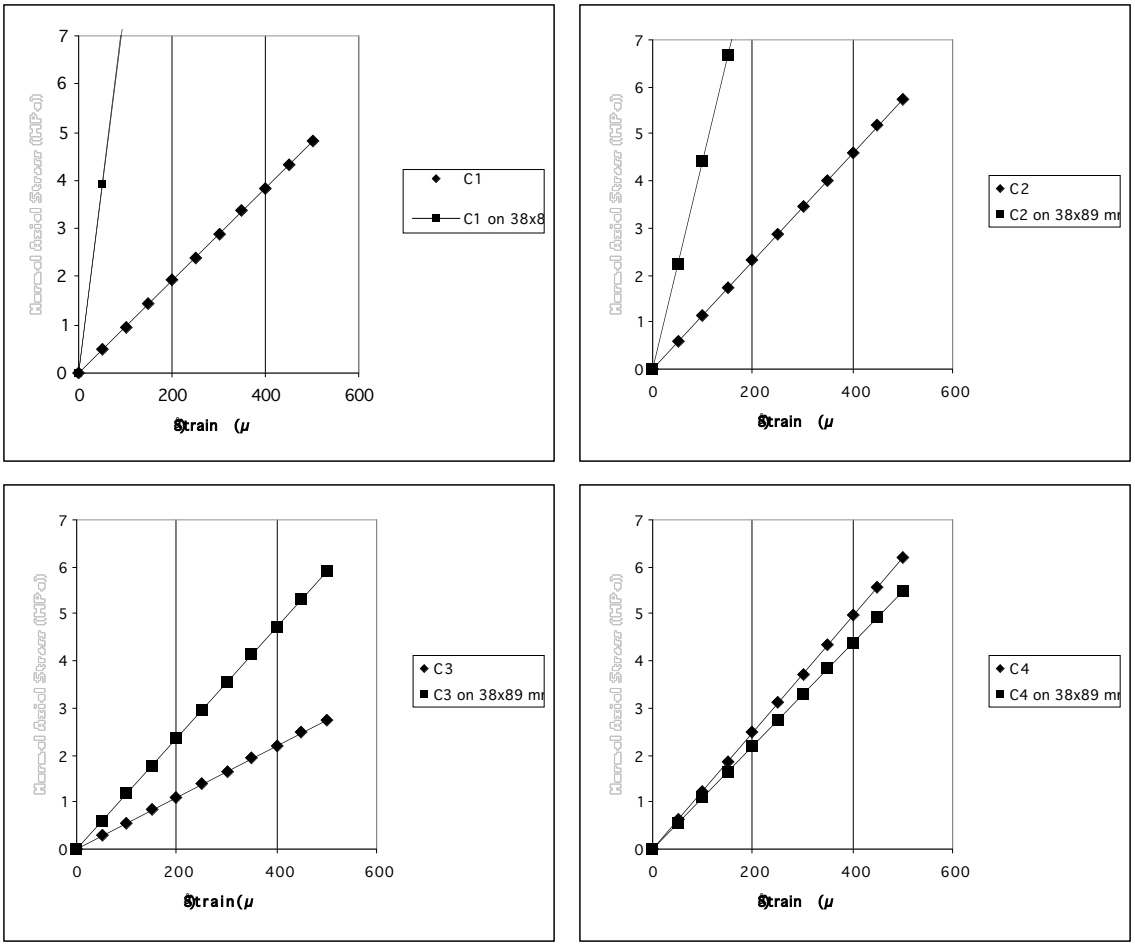

Fig. 4.18. The slope variation between the calibration and structural phase of Treatment C

Similar to the results obtained from Treatments A and B, there does not appear to be any consistent correlation between the stress-strain curves developed during the calibration and structural phases (See Appendix B for data from Treatments A and B).

For example, if the average of the four slope ratios presented in Table 4.16 were used to calculate the forces in the structural members based on the strain results of the calibration phase for the gages in Treatment C, the values produced in Table 4.16 would result. It is

apparent that these results are not within an acceptable tolerance of the actual member forces that produce these strain values.

Table 4.16. A comparison of the actual member forces to the predicted force based on the average slope ratio.

Strain (με)	Member Force for Gage C1 (kN)		Member Force for Gage C2 (kN)		Member Force for Gage C3 (kN)		Member Force for Gage C4 (kN)	
	Calc	Actual	Calc	Actual	Calc	Actual	Calc	Actual
25	1.5	6.6	1.8	3.8	0.9	1.0	2.0	0.9
50	3.0	13.2	3.7	7.5	1.8	2.0	4.0	1.8
100	6.0	26.4	7.4	15.0	3.6	4.0	8.0	3.6

Based on these findings, it was decided to repeat the experimental procedures of Treatment A, B, and C with a homogenous material of consistent physical properties. For Treatment D, acrylic was selected as the material for use during the specimen calibration phase.

Summary of Treatment A, Treatment B, and Treatment C

Throughout Treatments A, B, and C, metal foil strain gages were mounted on wood specimens of various sizes and subjected to loading of known magnitudes for the purposed of developing stress-strain curves for each specimen. This was termed as a "calibrated wood strain gage". Each calibrated wood strain gage was then mounted onto a one metre long piece of 38 x 89 mm dimensional lumber and subjected to loads of known magnitude. Stress-strain curves were then generated for the strain results given by the calibrated wood strain gage and compared to the curves generated in the calibration phase. It was hypothesized that a correlation should exist between the two stress-strain curves, which if known and consistent would allow for calculation of stresses in existing

structural members. In other words, the aim was to develop a system of non-destructive evaluation of existing wood framed structures.

Unfortunately, Treatments A, B, and C did not produce the results anticipated and a consistent correlation factor was not found. Several factors are known to have attributed to this conclusion, and other factors could possibly have contributed to this conclusion. Of primary importance in the experimental method was ensuring that consistent specimen preparation, experimental methods, and data analysis were undertaken. However, several factors contributed to inconsistencies throughout the experiment that negatively affected the results. These factors include difficulty handling small specimen sizes, heterogeneous anisotropic physical properties of a biological material, and difficulty performing quality assurance procedures. In addition to the difficulties created by wood's variable physical properties, its opaque nature severely limited our capability to determine the strength and adequacy of the bond between the strain gage and the wood specimen, as well as the bond between the wood specimen and the 38 x 89 mm piece of wood. It was our hope that the use of a material such as acrylic in Treatment D would alleviate some of these concerns and reduce the number of variables affecting the outcome of our experiment.

4.3.5 Treatment D

Treatment D consisted of mounting six strain gages on acrylic specimens with dimensions of approximately 3 x 25 x 75 mm. Table 4.17 details the exact dimensions of each specimen. Figure 4.19 indicates the stress-strain curves that resulted from the

calibration phase of the strain gages, and Table 4.19 indicates the equation of the best-fit linear regression trend line and the associated R^2 value.

Table 4.17. Dimensions of the specimens tested in Treatment D

Gage	Length (mm)	Width (mm)	Thickness (mm)
D1	77.7	23.9	2.9
D2	75.5	27.4	2.9
D3	76.4	24.5	2.9
D4	76.4	25.4	2.9
D5	76.2	24.4	2.9
D6	74.9	23.9	2.9

The acrylic specimens were subjected to compression forces. Table 4.18 indicates that the maximum force that each acrylic specimen was subjected to was less than the calculated compressive resistance of each specimen. The compressive capacity calculation used a specified compressive strength of 100 MPa for the acrylic based on published data for cast acrylic (MatWeb 2006).

Table 4.18. The factored compressive capacity of Treatment D specimens and the factored compressive load.

Gage	Compressive Capacity (kN)	Factored Maximum Axial Compression Force // to Grain (kN)
D1	7.5	0.3
D2	7.5	0.5
D3	7.5	0.4
D4	7.5	0.6
D5	7.5	0.5
D6	7.5	0.9

Treatment D used acrylic gages so that the quality of the bond between the acrylic specimen and the 38 x 89 mm member could be determined. In addition the

homogeneous nature of acrylic was being relied upon to produce more consistent measurements between different samples.

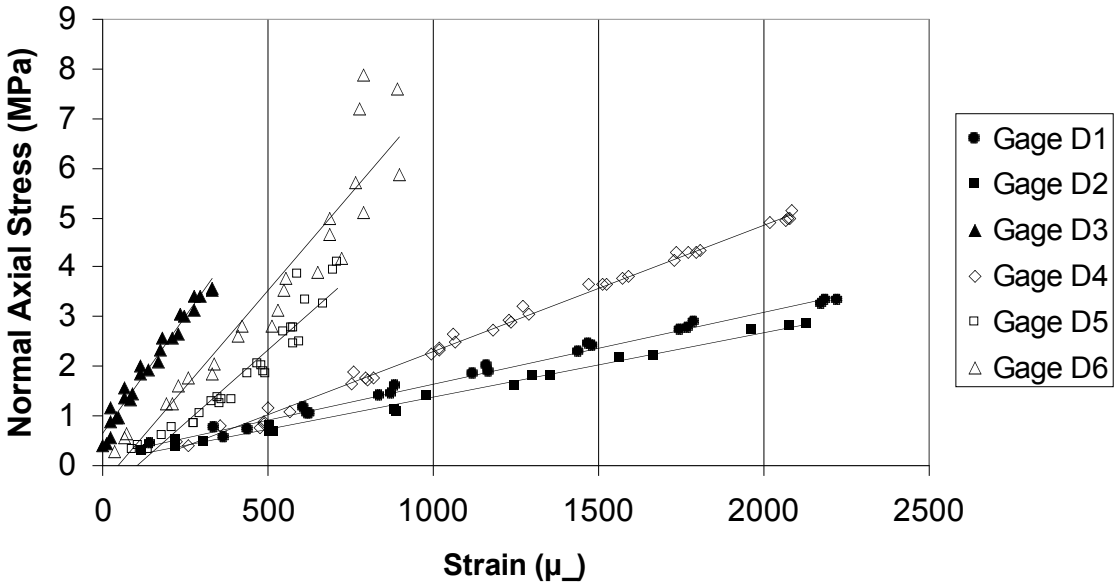

Fig. 4.19. The stress-strain curves for calibration phase of Treatment D

Table 4.19. The stress-strain curves and regression coefficients for the calibration phase of Treatment D.

Gage	Equation of Curve	R^2 Value
D1	y = 0.0014x + 0.2078	0.9915
D2	y = 0.0013x + 0.0951	0.9956
D3	y = 0.0095x + 0.626	0.9687
D4	y = 0.0026x - 0.2356	0.9952
D5	y = 0.0059x - 0.6366	0.9127
D6	y = 0.0078x - 0.3715	0.8933

The data collected for gage D3 included fluctuating strain levels for increasing stress and therefore was determined not to be operating properly. Inspection of the bond quality of the metal foil gage to the acrylic specimen indicated that a poor bond was a possible explanation for the unexpected results.

While more consistency was expected for the stress-strain curves of the six specimens, it is acknowledged that the variance in cross sectional areas between each specimen could account for some of the variance in results. The structural phase of Treatment D produced the results indicated in Figure 4.20 and Table 4.20. Figure 4.21 shows the relationship between the best-fit linear regression lines of the calibration and structural phase for each gage.

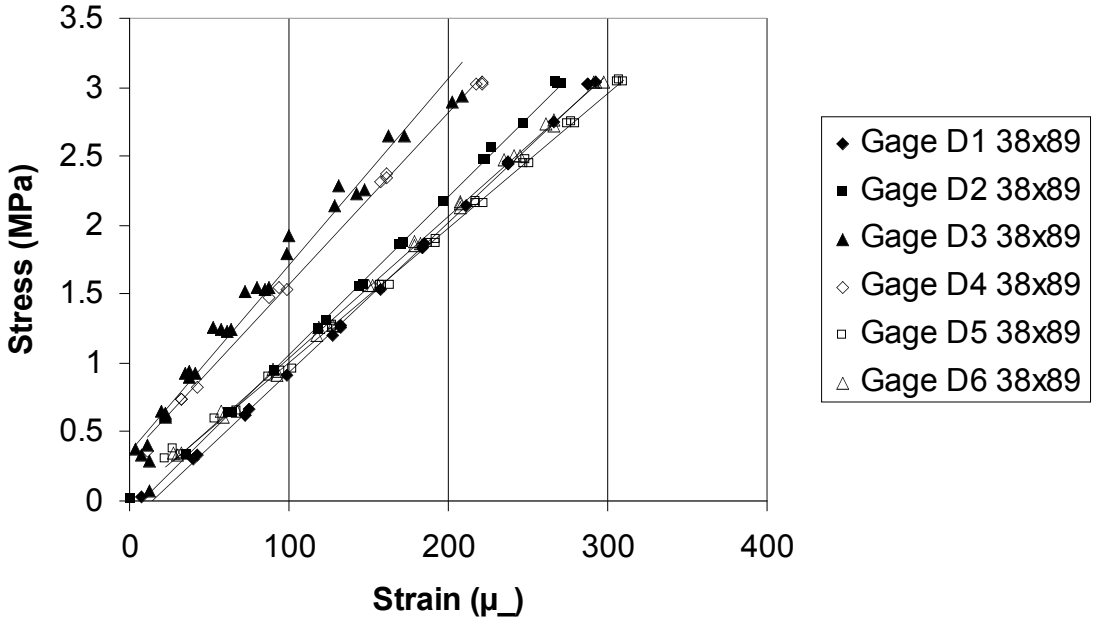

Fig. 4.20. The stress-strain curves for structural phase of Treatment D

Table 4.20. The stress-strain curves and regression coefficients for the structural phase of Treatment D, and the ratio between the slopes of the structural phase curve and the calibration phase curve.

Gage	Equation of Curve	R^2 Value	Ratio of Slopes
D1 on 38x89mm	y = 0.0109x - 0.1423	0.9989	0.13
D2 on 38x89mm	y = 0.0115x - 0.0904	0.9989	0.11
D3 on 38x89mm	y = 0.0136x + 0.3464	0.9705	0.70
D4 on 38x89mm	y = 0.0125x + 0.319	0.9977	0.21
D5 on 38x89mm	y = 0.0097x + 0.0262	0.9985	0.61
D6 on 38x89mm	y = 0.0103x + 0.0012	0.9986	0.76

In this test all replications produced linear stress-strain curves with high R^2 values. Interestingly Gages D1, D2, D5, & D6 produced similar curves, while gages D3 & D4 produced curves similar to each other but different from the other four gages.

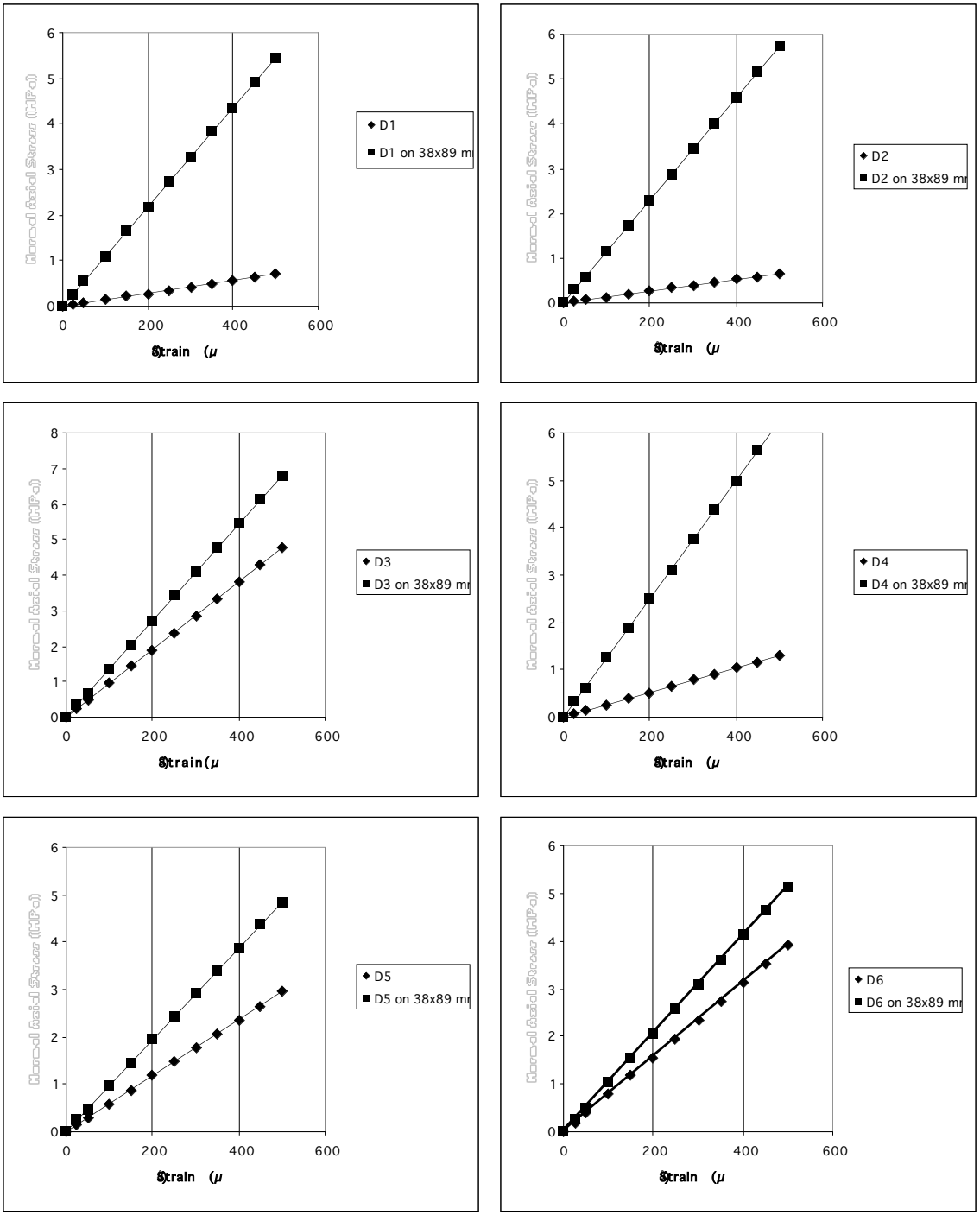

Fig. 4.21. The slope variation between the calibration and structural phase of Treatment D

There are two distinct groupings of consistent slope ratios: Gage D1, D2, & D4 and Gage D3, D5 & D6. All six gages were subjected to identical experimental conditions,

therefore the most likely contributing factor to the difficulty in creating reproducible results is the quality of the bond between the acrylic and the 38 x 89 mm. Figure 4.22 shows that there was not complete bond between the acrylic specimen and the 38 x 89 mm member for some of the gages.

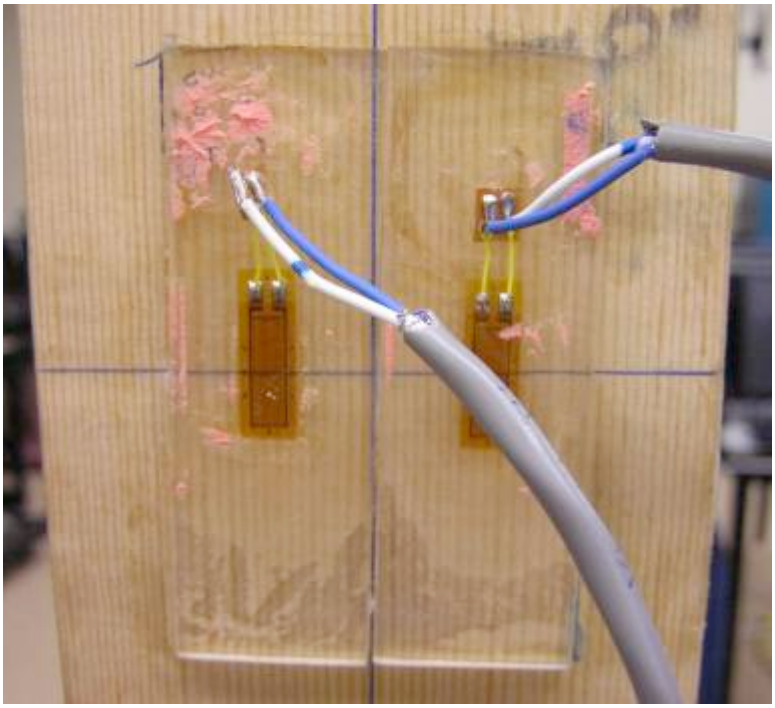

Fig. 4.22. The transparent nature of the acrylic specimens reveals an incomplete bond between the acrylic and the wood.

Another possible source of error that has been previously discussed is the difficulty in duplicating each replicate of the experiment under identical conditions. The large variation in stress-strain curves during the calibration phase of the acrylic specimens suggests that experimental conditions were not identical from between replications, and that there were possibly some errors in strain gage mounting.

Table 4.21 indicates that there is insufficient consistency in the slope ratios to use these results for measuring structural performance. For example, if the average of the six slope ratios presented in Table 4.21 were used for to calculate the forces in the structural members based on the strain results of the calibration phase for the gages in Treatment D, the values produced in Table 4.21 would result. It is apparent that these results are not within an acceptable tolerance of the actual member forces that produce these strain values.

Table 4.21. A comparison of the actual member forces to the predicted force based on the average slope ratio.

Strain (με)	Member Force for Gage D1 (kN)		Member Force for Gage D2 (kN)		Member Force for Gage D3 (kN)	
	Predict	Actual	Predict	Actual	Predict	Actual
25	0.28	0.95	0.26	0.97	1.91	1.15
50	0.56	1.90	0.52	1.94	3.82	2.00
100	1.12	3.80	1.04	3.88	7.64	4.00
	Member Force for Gage D4		Member Force for Gage D5 (kN)		Member Force for Gage D6 (kN)	
	Predict	Actual	Predict	Actual	Predict	Actual
25	0.52	1.05	1.19	0.82	1.57	0.87
50	1.04	2.10	2.38	1.64	3.14	1.74
100	2.08	4.20	4.76	3.28	6.28	3.48

It warrants repeating that the stress-strain curves for all six gages when mounted on the 38 x 89 mm wood specimen are relatively similar. A possible explanation is that the accuracy that is present during the calibration phase is lost during the process of bonding the acrylic onto the 38 x 89 mm wood piece, and that there is poor stress transmission through the 5 Minute® Epoxy. It is possible that there is a shear lag effect through the 5 Minute® Epoxy and that the dynamic nature of the test procedure did not allow sufficient time for the full stress effect of the applied load to propagate through the 5 Minute®

Epoxy bond to the surface of the strain gage. Additional work beyond the scope of this project will be required to further investigate this effect.

The reproducibility of the data, does however, increase when the results for Gages D3, D5, and D6 are removed from the analysis based on their unexpected and unusual behaviour during the calibration phase. As shown in Table 4.22, the actual and predicted member force values show much closer agreement than in Table 4.19, which further enhances the position that there is justification for further research into this technique.

Table 4.22. A comparison of the actual member forces to the predicted force based on the modified average slope ratio.

Strain (με)	Member Force for Gage D1 (kN)		Member Force for Gage D2 (kN)		Member Force for Gage D4	
	Predict	Actual	Predict	Actual	Predict	Actual
25	0.23	0.28	0.22	0.29	0.43	0.31
50	0.47	0.55	0.43	0.58	0.87	0.63
100	0.93	1.10	0.87	1.15	1.73	1.25

4.3.6 Statistical Analysis

The results of the statistical analysis completed for all four treatments are reproduced in Table 4.23. The results indicate that the standard deviations for the slope ratios are 58, 106, 97, 72, and 33 percent of the mean values for Treatment A, B, C, D, and D adjusted, respectively. In terms of load variance, these results translate into a variance of two orders of magnitude or more due to the wide distribution of measure values (wide, flat bell curve) associated with the calculated means and standard deviations. Therefore the treatments did not produce a consistent correlation between the performance of the gage

during calibration and the performance of the gage when mounted on the 38 x 89 mm member.

Table 4.23. The statistical analysis results for the ratios between calibration and structural slopes for each treatment.

Treatment	Mean	SD
A	0.22	0.13
B	3.83	4.05
C	0.53	0.51
D	0.42	0.30
D adjusted	0.15	0.05

4.4 Conclusions

An experimental program was designed with the intent of developing a new, practical approach to non-destructive evaluation of light-framed buildings. Of particular interest was the stress-strain relationship of wood members. It was believed that conventional metal foil resistance strain gages could be mounted onto wooden, and subsequently acrylic, specimens in a lab setting and that stress-strain relationships for these specimens could be determined based on physical measurement and observance of stress and strain levels. Once this calibration phase was completed, these new gages would be installed onto a larger structural member and the stress-strain relationship for that member could be determined. Ideally, a consistent correlation factor would exist between these two curves, and that correlation could be used to calculate the stress level in existing structural members based on the strain reading provided by the calibrated gages. Three different configurations of wood and one configuration of acrylic were used for the development of calibrated gages.

Treatment A investigated the performance of calibrated wood gages with dimensions of approximately 5 x 13 x 40 mm. There was great difficulty handling these specimens due to their small size, and the experiment was unsuccessful in achieving repeatable results. As a result, larger specimens of 100 x 40 x 5 mm were studied in Treatment B. These specimens showed more consistency in the calibration phase, but produced large variations in stress-strain curves when mounted on the 38 x 89 mm member. Treatment C studied the effects of specimen dimensions of 50 x 20 x 2mm. It was hoped that the narrower cross section would decrease the possibility for creep losses and stress relaxation through the thickness of the specimen when mounted on the 38 x 89 mm member. The results of Treatment C showed some reproducibility between both the calibration data and the stage two testing data, however the strength of the correlation between the two was not sufficient to give confidence in their values.

Based on the results and observations recorded for Treatments A, B, and C, it was determined that an alternate material source should be investigated for the calibration phase. As such, Treatment D used 75 x 25 x 3 mm specimens of acrylic. Acrylic was selected for its homogeneous properties, and transparent nature. It was believed that additional quality assurance related to assessing the quality of both the strain gage bond and the bond of the acrylic to the 38 x 89 mm member would be afforded due to the acrylic's transparency. A thickness of 3 mm was selected to coincide with the thickness of the wood specimens in Treatment C based on its better success. A thickness of 3 mm also provided the necessary stiffness for undergoing cyclical loading.

The results of Treatment D showed good correlation between two groups of three of the specimens investigated. It is believed that with additional refinement of the test method that ensures duplication of experimental conditions, the calibrated acrylic gages hold promise for application as a non-destructive evaluation technique.

The four research treatments did not produce a product that could be relied upon for real time monitoring or non-destructive evaluation of light-frame buildings. The research was, however, successful in developing a methodology that can be used for testing other materials and configurations for the development of calibrated wood strain gages. The biggest question regarding the outcome of this research program is why the stress at the surface of the structural specimen was not transmitted to the surface of the calibrated specimen at the location of the strain gage in a consistent manner. The most likely reason is inconsistency and inadequacy of the bond between the two wood specimens, and therefore more investigation of its physical properties is required. Using acrylic materials for the calibration phase of the testing appears to hold the most promise for successfully accomplishing the goals of this research.

5.0 SUMMARY

Light-framed buildings and in particular structures constructed with heterogeneous anisotropic materials present unique structural design, modelling, and non-destructive evaluation challenges. Particularly difficult is carrying out structural health monitoring on a practical level and in real world situations. This research project embarked upon developing a low cost, user friendly, practical non-destructive evaluation technique that could be used to determine stress and strain levels of structural members in light-frame buildings, with a particular focus on post-frame buildings.

A study of post-frame buildings including a comparison of their design to a regulatory analysis and a structural model indicated that the conventionally accepted post-frame construction technique does not comply with building code requirements. Some of the intricacies of the post-frame design are not adequately accounted for in current design and analysis techniques, and therefore a need for more research into the performance of these types of buildings was identified. The focus of this project was to fulfill that need with the development of a non-destructive evaluation technique that accurately measured stress and strain levels in wood building materials.

The non-destructive evaluation technique consisted of two parts. Part one was the calibration phase, in which metal foil resistance strain gages were mounted onto three different sizes of wood specimens, and one size of acrylic specimen, and were subsequently subjected to the application of known loads using a universal test machine. A stress-strain curve was developed for each specimen during this calibration phase. Part

two was called as the structural phase. It consisted of mounting the calibrated wood and acrylic gages onto a one metre piece of 38 x 89 mm dimension lumber which represented a typical light-framed building material. This assembly was then subjected to a similar loading program as described for part one, and the applicable stress-strain curves were developed.

A comparison of the stress-strain curves developed for the two parts of the research program was completed to determine if a consistent correlation existed between the slopes of the two curves. The results indicated that the calibration gages for the wooden specimen provided no appreciable consistency, while the results for the acrylic gage showed the possibility of a weak correlation. In either case the variance in the results of the testing could lead to over and/or under estimation of loads by two orders of magnitude or more. Therefore, the results can not be relied upon for predicting or measuring loads in structural members.

The research program concluded that additional evaluation of acrylic as the material for the calibration phase is necessary to determine if its use will lead to the successful development of the desired non-destructive evaluation technique. The project identified several possible areas of improvement and refinement of the experimental method that will increase the likelihood for success.

Finally, this project concluded that there remains a strong need for a practical structural health monitoring technique for light-framed structures, and found there to be strong promise in the use of metal foil resistance strain gages as the basis for this system.

6.0 RECOMMENDATIONS FOR FURTHER STUDY

Although this research project did not achieve its stated objective, it was successful in developing a research method appropriate for the evaluation of a specific non-destructive evaluation technique for biological materials. Further refinements of this method will aid in the construction of practical, accurate strain measurement technique applicable to light-framed buildings. The following list of recommendations is based on the writer's experience throughout this research project, and will serve as a basis for future improvements to the research method.

1. Additional investigation of the performance of acrylic as the calibration gage material including different sizes will determine if acrylic specimens are indeed the key to the success of the project.
2. Evaluation of the 5 Minute® Epoxy as a bonding agent should be completed to determine if its continued use is appropriate. It is recommended that the epoxy bond's performance be studied under controlled conditions with physical materials of known properties in order to evaluate its effectiveness.
3. Further refinement of the experimental method including more advanced and precise apparatus and data acquisition equipment will increase the accuracy and precision of observed and recorded results.
4. Different sizes of metal foil resistance strain gages should be studied to determine what, if any, the effect of using different gages is on the experimental results.
5. The development of a system that allows for the re-use of a calibrated gage should be investigated. For example, a small specimen of stainless steel or aluminum

could be use as the calibration specimen and then attached to the structural member. This type of assembly could then be removed and attached to a different structural specimen for additional testing.

6. Experimental lab results should be compared to results obtained from evaluation of structural members in existing research buildings.
7. Once this non-destructive evaluation technique is perfected, the results obtained from its implantation should be used to revise and improve design and modelling techniques for light-framed buildings.
8. Maintain the research focus on the development of a practical, low cost system that is capable of performing the required structural health monitoring in real world situations.

7.0. REFERENCES

Atkinson, D. and G. Hayward. 2001. Active Fibre Waveguide Sensor for Embedded Structural Condition Monitoring. *IEEE Proceedings*. 148(4). 160-168.

Beards, C.F. 1983. *Structural Vibration Analysis: Modelling, Analysis and Damping of Vibrating Structures*. Chichester, England: Ellis Horwood Limited.

Bohnhoff, D.R. 1992. Expanding Diaphragm Analysis for Post-Frame Buildings. *Trans. ASAE*. 8(4): 509-517.

Bohnhoff, D.R., G.A. Anderson and N.F. Meador. 1990. Simplified Three-Dimensional Analysis for Post-Frame Buildings. ASAE Paper No.904032. St. Joseph, Mich.: ASAE.

Carmichael, D. G. 1981. *Structural Modelling and Optimization*. Chichester, England: Ellis Horwood Limited.

Cawley, P. and R.D. Adams. 1979. The Location of Defects in Structures From Measurements of Natural Frequencies. *Journal of Strain Analysis*. 14(2) 49-57.

Chalmers, G.F. 1982. Materials, Construction, Performance and Characteristics. In *Strain Gauge Technology,* 1-38. London, U.K.: Applied Science Publishers.

Chance, B. H. and D.E. Bray. 2002. Nondestructive Monitoring of Stress Relaxation in Welded Steel Plates. *Journal of Pressure Vessel Technology* Vol. 124 343-348.

Chen, W. and A.F. Saleeb. 1982. *Constitutive Equations for Engineering Materials*. Toronto, Ontario: John Wiley & Sons, Inc.

Cullington, D.W. and C. Beales. 1977. Residual Stresses and Distortions Measured During Construction of the Milford Haven Bridge. *Journal of Strain Analysis*. 12(2). 123-129.

CSA O86-01. 2005 Engineering Design in Wood (Limit States Design) Structures (Design). Etobicoke, Ontario.: Canadian Standards Association.

CWC. 1999. Introduction to Wood Design. CWC 1999 Edition. Ottawa, Ontatio.: Canadian Wood Council.

CWC. 1995. Wood Design Manual 1995. CWC Ottawa. Ontario.: Canadian Wood Council

Dally, J.W. 1965. *Experimental Stress Analysis*. New York, N.Y.: McGraw Hill

Dym, C.L. 1997. *Structural Modelling and Analysis*. Cambridge, UK: Cambridge University Press

Elezaby, Y.K. and S.H. Simmonds. 1992. Modelling and design of unbraced reinforced concrete frames. Report No. 175. Edmonton, Alberta.: University of Alberta

Esin, A 1980. Prediction of the Cyclic Hardening Stress-strain Curve. Journal of Strain Analysis. 15(4). 235-237.

Fessler, H. 1977. Applications of Photoelasticiy. *Methods and Practice for Stress and Strain Measurement*. 57-62. British Society for Strain Measurement.

Fessler, H. and W.J.G. Little. 1981. Elastic Stresses Due To Axial Loading of a Two-Brace Tubular K Joint With and Without Overlap. *Journal of Strain Analysis*. 16(1). 67-77.

Fessler, H. and P.J. Woods. 1982. Stress Concentrations on Axially Loaded, Unsymmetrical Projections on Flat Bars. *Journal of Strain Analysis*. 17(1). 23-29.

Fukumoto, Y. and G.C. Lee. 1992. *Stability and Ductility of Steel Structures Under Cyclic Loading*. Boca Raton, Florida: CRC Press, Inc.

Giurgiutiu, V., A. Zagrai and J. Bao. 2002. Embedded Active Sensors for In-Situ Structural Health Monitoring of Thin-Wall Structures. *Journal of Pressure Vessel Technology*. 124. 292-302.

Harms, K. D. and C.S. Suh. 2002. Laser-Optic Evaluation for Bond Quality of Polymeric Medial Tubing. *Journal of Pressure Vessel Technology* Vol. 124 283 292.

Irish, W. W., R.A. Parsons and G.D. Wells. 1976. *Pole and post building construction.* NRAES-1. Ithica, NY: Northeast Regional Agricultural Service.

Khan, A.S. and X. Wang. 2001. *Strain Measurements and Stress Analysis*. Upper Saddle River, N.J.: Prentice Hall

Kratzig, W. B., O.T. Bruhns, H.L. Jessberger, K. Meskouris, H.J. Niemann, G. Schmid, F. Stangenberg, A.N. Kounadis. and G.I. Schueller. 1991. *Structural Dynamics* Rotterdam, Netherlands: A.A. Balkema.

Lardner, T. J. and R.R. Archer. 1994. *Mechanics of Solids, An Introduction*. Highstown, N.J.: McGraw-Hill.

Madsen. 1992. Structural Behaviour of Timber. *Timber Engineering Ltd*. North Vancouver, B.C.

Mahmud, M. B. and T.F. Zimmie. 1998. Instrumentation and Calibration of Geotextiles Used in Centrifuge Modelling of Slopes. *Transportation Research Record*. 1614. 3-7.

Manbeck, H. B., N.F. Meador and G.L. Nelson. 1988. *Light Agricultural and Industreatment Structures Analysis and Design,* New York, NY: Van Nostrand Reinhold Company Inc.

Martin, W.N., A. Ghoshal, M.J. Sundaresan, G.L. Lebby, M.J. Shulz and P.R. Pratap. 2002. Artificial Nerve System for Structural Monitoring. *Proceedings of SPIE*. 4702. 49-62.

Margetson, J. 1981. Tensile Stress/Strain Characterization of Non Linear Materials. *Journal of Strain Analysis*. 16(2). 107-111.

MatWeb. 2006. Material Property Data. Available at www.matweb.com. Accessed Nov. 4, 2006.

Miles, A.W. and K.E. Tanner. 1992. *Strain Measurement in Biomechanics*. New York, N.Y.: Chapman and Hall

Miyasaka, C., B.R. Tittmann and S. Tanaka. 2002. Characterization of Stress at a Ceramic/Metal Joined Interface by the V(z) Technique of Scanning Acoustic Microscopy. *Trans. ASME* Vol. 124 336 – 342.

Mordan, G.C.. 1982. Adhesives and Installation Techniques. In *Strain Gauge Technology*. 39-83. London, U.K.: Applied Science Publishers.

Na, W. and T. Tribikram. 2002. EMAT-Based Inspection of Concrete-Filled Steel Pipes for Internal Voids and Inclusions. *Journal of Pressure Vessel Technology*. Vol 124 265-272.

Pople, J. 1982. Errors and Uncertainties in Strain Measurement. In *Strain Gauge Technology*. 209-264. London, U.K.: Applied Science Publishers.

Procter, E. 1977. Strain Gauge Practice. *Methods and Practice for Stress and Strain Measurement*. 5-11. British Society for Strain Measurement.

Randolph, M.F. and E. Lightfoot. 1975. Analysis of Strain-Gauge Data From Thin-Walled Structural Members Subjected to Eccentric Longitudinal Loading. *Journal of Strain Analysis*. 10(2). 104-110.

Scott, K. and A. Owens. 1982. Instrumentation. In *Strain Gague Technology*. 139-207. London, U.K.: Applied Science Publishers.

Soden, P.D. and R.D. McLeish. 1976. Variables Affecting the Strength of Balsa Wood. 1976. *Journal of Strain Analysis*. 11(4). 225-234.

Stanley, P. 1977. Basic Photoelastic Theory and Polariscope Techniques. *Methods and Practice for Stress and Strain Measurement*. 35-43.British Society for Strain Measurement.

Towle, J.E. and V.L. Dutton. 1967. Instruction Manual for Tuckerman Strain-Gage Apparatus. University of Manitoba Department of Civil Engineering. CE-1-67. Winnipeg, Manitoba.

Vishay Micro-Measurements. 2005. Strain Gage Applications with M-Bond AE-10, AE-15 and GA-2 Adhesive Systems. Vishay Instruction Bulletin B-137. Shelton, CT.: Vishay Micro-Measurements.

Walker, J.N. and F.E. Woeste. 1992. *Post-Frame Building Design,* St. Joseph, MI: American Society of Agricultural Engineers.

Wang, W.,J. Dee, W. Ledoux, B. Sangeorzan and P. Reinahll. 2002. Development of a Directional Sensitive Pressure and Shear Sensor. *Proceedings of SPIE*. 4702. 212-221.

Yettram, A.L. 1989. *Mechanical Properties and Stress Analysis in Biomechanics*. New York, N.Y.: Manchester University Press.

APPENDIX A

A.0 STRUCTURAL MODELLING OF A POST-FRAME BUILDING

A.1 Introduction

This appendix serves as a companion piece to the research report as it further develops the rationale for investigating new structural design and analysis techniques for light-framed buildings, including post-frame buildings.

The complexities of the relationships between the different structural elements of the post-frame building are not adequately captured in conventional design procedures and in the computer modelling software. Therefore, more information is required regarding measured structural performance of post-frame buildings under various load conditions. System design including the consideration of diaphragm action on load transfer and re-distribution requires understanding when evaluating the performance of post-frame buildings. The ability of wood frame buildings to act as a system whose overall building strength is greater than the sum of its individual parts is a benefit of wood construction that is not captured in conventional design techniques.

Structural modelling is a valuable tool available to structural engineers that allows for the prediction of a building's structural performance under different designs and load cases. Computer based models have increased the speed and efficiency with which engineers can test different building configurations and different building materials to determine their effectiveness in satisfying the building objectives. The following describes the development of a RISA-3D structural model of a post-frame straw bale building at the University of Manitoba. A comparison of this model to the expected performance of the

building based on accepted structural engineering principles will outline some of the difficulties in predicting the performance of light-framed buildings.

A.2 Materials and Methods

A software based structural model of a post-frame building located at the University of Manitoba in Winnipeg, MB was created using the RISA-3D software program and a personal computer. RISA-3D is structural engineering and analysis software that is intended for the design and analysis of general frame, truss, and shell or plate structures.

Concurrently, structural analysis was completed for the post-frame building to determine the load resistance requirements of the structural members according to the National Building Code (NBCC 1995). These results were then compared to the results calculated by the computer model.

A.2.1 Building Design and Construction

The subject building is a 32.6 m long, 12 m wide, 6 m high post-frame building. The wall design is shown in Fig. A.1, which indicates a straw bale wall with laminated 3 ply 38 mm by 184 mm pressure treated posts at a spacing of 2.15 m on centre. The post installation in the ground is shown in Fig. A.2, and shows the posts extending 2.6 m below grade, with concrete placed into the bottom 0.75 m of the hole. The roof of the building is designed as an engineered wood truss system, and the straw bale walls are supported by a concrete footing that incorporates straw bale walls into its design as shown in Fig. A.3.

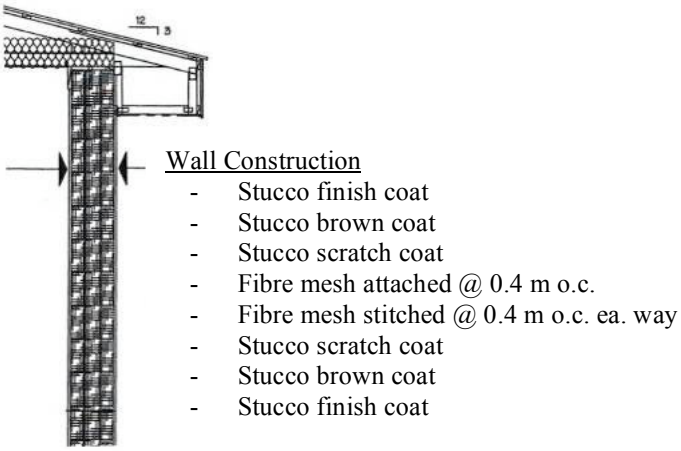

Fig. A.1. The wall profile of a straw bale building showing the material and installation methods that will be used. (Building Alternatives Inc., Drawing # S1, 2003) Used with permission from Building Alternatives Inc., May 7, 2007

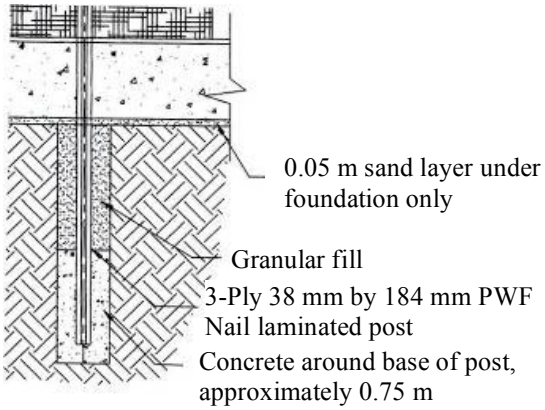

Fig. A.2. A cross section of the post installation in the ground. (Building Alternatives Inc. Drawing #S3 , 2003) Used with permission from Building Alternatives Inc., May 7, 2007

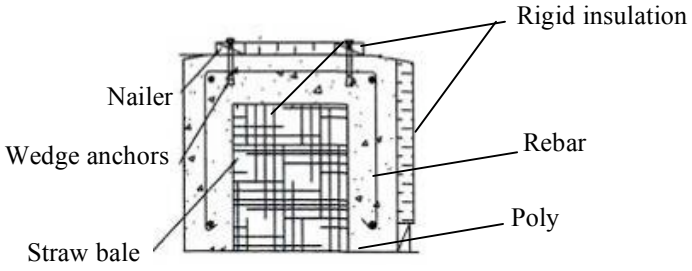

Fig. A.3. A cross section of the footing design indicating a U-shaped concreted footing poured over top of straw bales wrapped in poly. (Building Alternatives Inc. Drawing #S3 , 2003) Used with permission from Building Alternatives Inc. May 7, 2007

All of the physical members of the post-frame building, with the exception of the alternative foundation design, were included in the structural model. The wall and roof sheathing were modelled as shells. The fact that the post-frame building consists of straw bale walls with a stucco finish created an added level of complexity and uncertainty in the model design. In the case of this modelling scenario it was felt that modelling the outside walls as a plywood sheathed wall would provide sufficient information with regard to loads in the lateral structural system.

A.2.2 Testing Equipment and Experimental Design

Testing equipment installed throughout the building include load cells attached to the top and bottom of selected posts, as well as type k thermocouples installed at the bottom of the same posts. The locations of these test posts are shown as open squares in Fig. A.4. Similar load cells are also installed at random points throughout the lateral truss bracing. The wall design also includes removable test panels that will facilitate the testing of different wall materials under different conditions. The test panel design is shown in Fig. A.5.

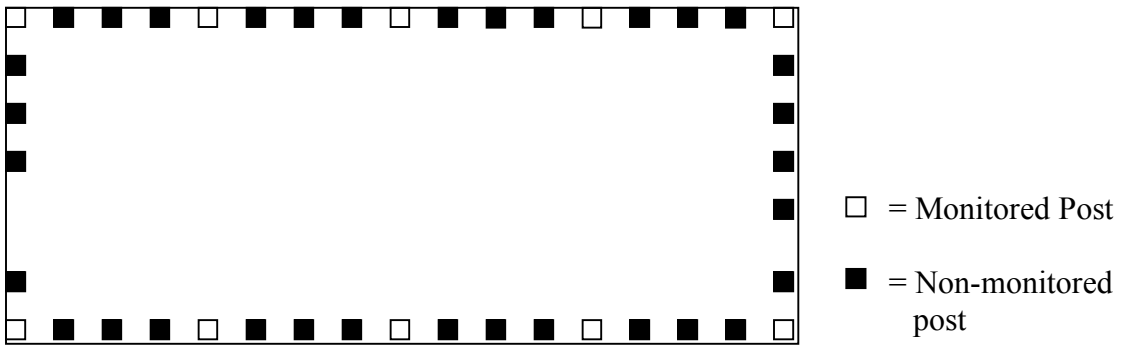

Fig. A.4. Post layout showing the location of the monitored posts.

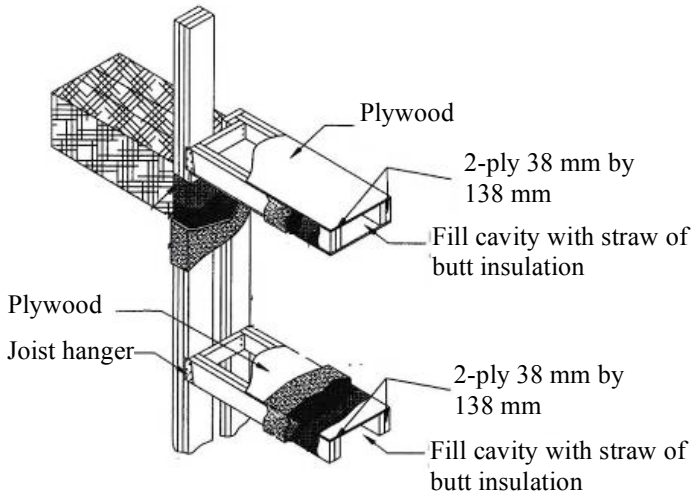

Fig. A.5. The framing details at the test panel location allow for the replacement of large sections of wall with different building material for testing. (Building Alternatives Inc., Drawing #S4, 2003) Used with permission from Building Alternatives Inc., May 7, 2007

A.2.3 Material Properties and Specifications

Due to the fact that RISA-3D is an American product, its default physical properties for structural materials are those specified by American codes. Normally this would not be a problem as American and Canadian codes usually have similar specifications, but in the case of the post-frame building under review this created a problem due to its wood construction. The accepted physical properties of wood required for use in Limit States Design by the Canadian Building Code were different than the default values in RISA-3D. Therefore, prior to analyzing the structure as modelled, it was necessary to modify the physical parameters and properties of the various wood members used in the construction of the post-frame building. Table A.1 shows the specified strength values assigned for the various structural members of the building for use in the RISA-3D database.

Table A.1. The specified strength values assigned to the various structural members for the RISA-3D model.

Element	Size (mm)	Specified Strengths (MPa)				Modulus of Elasticity E (MPa)	
		Bending	Tension // to Grain	Longitudinal Shear	Compression // to Grain	E	E_{05}
Posts	3 ply 38 x 184	11.8	5.5	1.0	11.5	9500	6500
Top Plate	38 x 235	11.8	5.5	1.0	11.5	9500	6500
LVL	38 x 235	25.6	20.4	2.0	30.2	12400	N/A
Bracing	38 x 89	11.8	5.5	1.0	11.5	9500	6500
Truss Webs	38 x 89	11.8	5.5	1.0	11.5	9500	6500
Truss Members	38 x 140	11.8	5.5	1.0	11.5	9500	6500
Purlins	38 x 89	11.8	5.5	1.0	11.5	9500	6500

A.2.4 Structural Analysis of the Posts

Certain design assumptions were made in order to facilitate the calculations required for structural analysis. All assumptions were based on the information contained in CSA O86-01. The specified bending strength, f_b, was taken as 11.5 MPa in accordance with Table 5.3.1A of O86-01 (CSA). The load duration factor, K_D, was taken as 1.15 since the duration of the loading during the experiment was less than seven days. The system factor, K_H was taken as 1.0 since the posts were space further than 610 mm apart. The service condition factor for compression K_{sc}, was determined to be 1.0, the factor for dry service conditions. The treatment factor K_T, was also taken as 1.0 since the posts were thicker than 89 mm. All other values and factors were determined in accordance with the applicable formulas and calculations.

The analysis of the building was completed using Limit States Design as required by the National Building Code. Factored loads were determined based on Equations A.1 to A.5,

and the factored resistances of the posts as designed were determined based on Equations A.5 to A.13. The total factored load was determined based on load case II for the snow load, and considering snow loads and wind loads acting at the same time. This represents the worst case scenario for the factored load.

Factored Loads

$F.L. = \alpha_D D + \varphi\gamma(\alpha_L L + \alpha_w W)$; **where** **Equation A.1**

$\alpha_D = Dead\ Load\ Factor = 1.25$

$D = Dead\ Load$

$\varphi = Load\ Combination\ Factor = 0.7$

$\lambda = Importance\ Factor = 1$

$\alpha_l = Live\ Load\ Factor = 1.5$

$L = Live\ Load$

$\alpha_w = Wind\ Load\ Factor = 1.5$

$W = Wind\ Load$

$D = Dead\ Load = Weight\ of\ Roofing\ Materials$ **; where** *Aluminum = 20 Pa*

Sheathing = 80 Pa

Trusses (Average over Building Area) =100 Pa

Insulation = 30 Pa

Total = 230 Pa,

use 0.25 kPa

D = 0.25 kPa

L = Snow Load = $S = S_s(C_b C_w C_s C_a) + S_r$ **; where** **Equation A.2**

$S = S_s(C_b C_w C_s C_a) + S_r$

$S_s = Ground\ Snow\ Load = 1.7$

$C_b = Basic\ Roof\ Snowload\ Factor = 0.8$

$C_w = Wind\ Exposure\ Factor = 1.0$ **Equation A.3**

$C_s = Roof\ Slope\ Factor = 1.0\ for\ case\ I, 1.05\ for\ case\ II$

$C_a = Accumulation\ Factor = 1.0$

$S_r = Associated\ Rain\ Load = 0.2$

$L = 1.7(0.8 \times 1 \times 1 \times 1) + 0.2 = 1.56\ kPa\ for\ case\ I$

$L = 1.7(0.8 \times 1 \times 1.05 \times 1) + 0.2 = 1.63\ kPa\ for\ case\ II$

W = Wind Load = $P = qC_e C_g C_p$ **; where** **Equation A.4**

$q = Reference\ Velocity\ Pressure = 0.42$

$C_e = Exposure\ Factor = 1.0$

$C_g C_p = External\ Peak\ \text{Pr}essure\ Coefficients = 2.0\ Maximum$

$W = 0.42 \times 1 \times 2 = 0.84\ kPa$

Figures A.6 and A.7 show the external peak pressure coefficients and the resulting wind loads at various locations on the building.

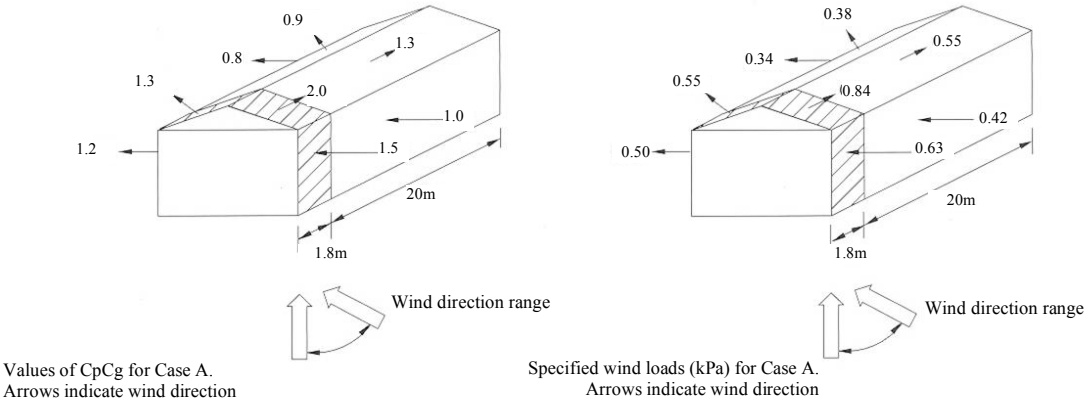

Values of CpCg for Case A.
Arrows indicate wind direction

Specified wind loads (kPa) for Case A.
Arrows indicate wind direction

Fig. A.6. The CpCg factors for side winds, and the resultant calculated wind loads.

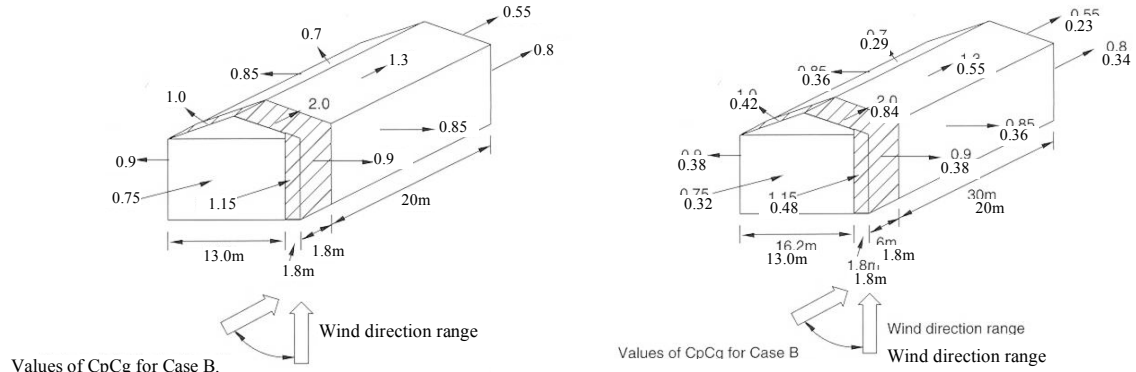

Values of CpCg for Case B.
Arrows indicate wind direction

Specified wind loads (kPa) for Case B.
Arrows indicate wind direction

Fig. A.7. The CpCg factors for end winds, and the resultant calculated wind loads.

The wind load generally causes uplift effects, and therefore it is not adding vertical load onto the posts. As a result, its effects are ignored for the remainder of the vertical post load calculation.

$$F.L. = 1.25(0.25) + 1 \times 0.7(1.5 \times 1.64) = 2.03\ kPa$$

$$F.L. = 2.03\ kPa$$

The maximum area supported by a post is 13 m^2, so the compression force acting on the post is 26.2 kN as calculated by equation A.5

$$P_f = F.L. \times Area = 2.03 \times 12.9 = 26.2\ kN \qquad \textbf{Equation A.5}$$

$$P_f = 26.2\ kN$$

Factored Load Resistance Requirements

$P_r = \phi F_c A K_{zc} K_c$ **; where** **Equation A.6**

$\phi = 0.8$

$$F_c = f_c(K_D K_H K_{sc} K_T) = 11.5(1 \times 1 \times 1 \times 1) = 11.5 \qquad \textbf{Equation A.7}$$

$$A = cross\ sectional\ area = 140 \times 184mm = 25760mm^2 \qquad \textbf{Equation A.8}$$

$$K_{zc} = 6.3(dL)^{-0.13} = 6.3(184 \times 6000)^{-0.13} = 1.03 \qquad \textbf{Equation A.9}$$

$$K_C = \left[1.0 + \frac{F_C K_{zc} C_c^{\ 3}}{35 E_{05} K_{SE} K_T}\right]^{-1} = \left[1.0 + \frac{11.5 \times 1.03 \times 34.3^3}{35 \times 5000 \times 1 \times 1}\right]^{-1} = 0.27 \qquad \textbf{Equation A.10}$$

$$C_c = {}^{L_e}\!/_{b}\ or\ {}^{L_e}\!/_{d} = {}^{6000}\!/_{140} = 34.3\ or\ {}^{6000}\!/_{184} = 26.1\ choose\ larger \qquad \textbf{Equation A.11}$$

$C_c = 34.3 < 50 \therefore OK$

$$L_e = K_e L = 0.8 \times 6.0 = 4.8 \qquad \textbf{Equation A.12}$$

$$P_r = \phi F_c A K_{zc} K_c = 0.8 \times 11.5 \times 25760 \times 1.03 \times 0.27 = 65.9\ kN$$

In accordance with clause 5.5.6.4.2 *for nailed built – up compression members*, *an additional factor of* 0.6 *shall be applied*, *therefore*

$$P_r = 65.9\ kN \times 0.6 = 39.5\ kN$$

Equation A.13

$$P_r = 39.5\ kN$$

The structural analysis has determined that the post design for the post-frame building provides adequate compressive resistance to the axial compressive loads that the post will be subject to. It follows that the combined effects of bending and compression on the structural posts must be considered. Equations A.14 to A.20 examine these combined effects.

$Total\ Moment = M_f = m'_f + P_f \Delta_T$ **; where** **Equation A.14**

$m'_f = Factored\ Moment\ due\ to\ Wind\ Load$

$P_f = Factored\ Axial\ Load$

$\Delta_T = Total\ Lateral\ Deflection$

$$m'_f = {wL^2}/{8} = {1.4(6)^2}/{8} = 6.3\ kN \bullet m$$ **Equation A.15**

$$P_f = 26.2\ kN$$

$$\Delta_T = \Delta_L \left[\frac{1}{1 - {P_f}/{P_E}} \right]$$ **; where** **Equation A.16**

$$\Delta_L = \frac{5 w_f L^4}{384 E_s I} = \frac{5 \times 1.4 \times 6000^4}{384 \times 5000 \times \frac{140 \times 184^3}{12}} = 65.0\ mm$$

$$P_E = Euler\ Buckling\ Load = \frac{\pi^2 E_s I}{(K_e L)^2} =$$

Equation A.17

$$= \frac{3.14^2 \times 5000 \times \frac{(140 \times 184^3)}{12}}{4800^2} = 155.7\ kN$$

$$\Delta_T = 76.4\left[\frac{1}{1 - 26.2/155.7}\right] = 78.2$$

$$\Delta_T = 78.2\ mm$$

$$M_f = m'_f + P_f \Delta_T = 6.3 + 26.2 \times .078 = 8.3$$

$$M_f = 8.3\ kN \bullet m$$

$M_r = Factored\ Moment\ Resistance = \Phi F_b S K_{zb} K_L$ **; where** **Equation A.18**

$\phi = 0.9$

$F_b = f_b(K_D K_H K_{Sb} K_T) = 11.0(1 \times 1 \times 1 \times 1) = 11.0$

$S = bd^2/6 = 140 \times 184^2/6 = 789973$ **Equation A.19**

$K_{zb} = 1.3$

$K_L = 1.0$

$$M_r = 0.9 \times 11.0 \times 789973 \times 1.3 \times 1.0 = 10.2$$

$$M_r = 10.2\ kN \bullet m$$

These calculations indicated that the total moment that the posts are subjected to is less than the moment resistance of the posts. The combined effects of the compression and bending forces on the posts are represented in equation A.20.

$$\frac{P_f}{P_r} + \frac{M_f}{M_r} = \frac{26.2}{39.5} + \frac{8.3}{10.2} = 1.5 \geq 1.0 \therefore \textit{not acceptable} \qquad \textbf{Equation A.20}$$

The analysis has determined that the post design for the post-frame building is sufficient to resist compressive and bending moment forces independently, however the combination of their effects exceed design criteria. Nonetheless, empirical evidence indicates that the post design is sufficient for the post-frame building. Structural modelling, non-destructive testing, and real time monitoring and evaluation of the post-frame building is required to determine if accepted structural design techniques are applicable to building systems such as those use in post-frame buildings.

A.2.5 Model Development

Owing to the symmetrical nature of the building along its z-axis (along the building length), it was possible to create individual sections of the building and use RISA-3D's mirroring, copying, and cloning tools to develop a model of the entire building. The steps used in the model development are described in the following.

1. Create a model of one individual truss, including nodes for purlin and lateral bracing attachment.
2. Copy and mirror the original truss to create a roof system consisting of 33 individual trusses at a spacing of 1.1 m on centre.

3. Add 38 x 89 mm purlins to the roof system perpendicular to the trusses. The purlins were added at a spacing of 600 mm on centre across the top cord of each truss and ran the entire length of the building.
4. Add 38 x 89 mm lateral bracing on the bottom cord of each truss at points three metres inside the wall connection. The bracing ran the entire length of the building.
5. Add 38 x 89 mm lateral bracing at the midpoint of the inside webs of each truss. The bracing ran the entire length of the building.
6. Add 38 x 235 mm wall top plate to the bottom cord of each truss at a point one metre from the outside toe of the truss, therefore creating a one metre roof overhang.
7. Add the 3 ply 38 x 184 mm (modelled as a 140 x 184 mm) structural posts to the model at a spacing of 2.15m on centre along the length of the building. Add the 3 ply 38 x 184 posts on the ends of the building according to the spacing required for door installations. The post to foundation connections were modelled as pins. An additional node was placed on each post at a point 2.4 metres from the bottom of the post to represent the location at which the post was exposed to the surface.
8. Add plywood sheathing to the roof and walls of the model.
9. Add additional details for specialized structural members, ie) LVL beams over garage door openings.

Figures A.8 to A.11 show the progression from component to module to building system beginning with the original truss, and ending with the complete building model.

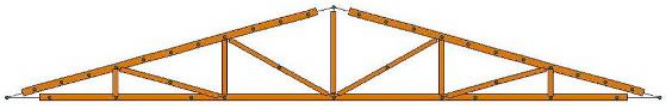

Fig. A.8. A modelled truss representing the trusses in use at the straw bale building.

Fig. A.9. The replication of the modelled truss representing the roof system at the straw bale building.

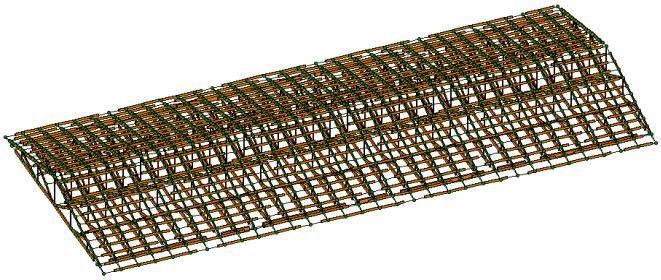

Fig. A.10. A model of the complete roof system including trusses, purlins, and bracing.

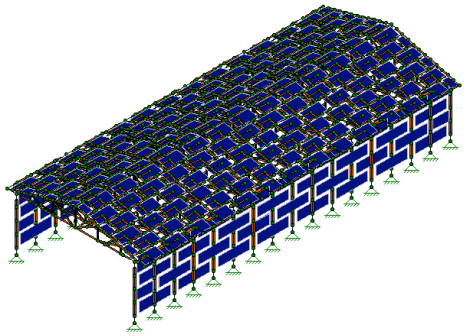

Fig. A.11. A complete model of the straw bale building including all structural elements and the roof sheathing.

A.2.6 Building Loads

In order to run the model the magnitude of the various loads had to be specified. The dead and live loads required calculations in accordance with the National Building Code to determine their expected magnitudes at the building location. Equations A.1 to A.5 detail these calculations.

A.2.7 Load Combinations

After establishing the physical properties of the structural members, various load combinations that were to be considered in the modelling process were determined. In accordance with the requirements of the National Building Code, the load combinations as detailed in Table A.2 were input into the computer model.

Table A.2 The various load cases considered in the model of the post-frame building.

Load Case	Loads Considered
1	Dead Load
2	Dead Load + Snow Load (Case I)
3	Dead Load + Snow Load (Case II)
4	Dead Load + Snow Load (Case I) + Wind Load (Case I)
5	Dead Load + Snow Load (Case I) + Wind Load (Case II)
6	Dead Load + Snow Load (Case II) + Wind Load (Case I)
7	Dead Load + Snow Load (Case II) + Wind Load (Case II)

A.2.8 Structural Performance and Behavioural Analysis

Once all of the necessary computer inputs had been determined and/or calculated and loaded into the model, the model was run for the various load combinations and its results were analyzed. For this study, the focus was on the performance of the main structural posts. The original intention was to compare the results of this computer based theoretical analysis, the predictive structural analysis, and the results obtained from non-destructive evaluation techniques using the strain measurement strategies developed in Section 4 of this thesis. However, due to the inability to create a method that was able to consistently predict stress levels based on strain measurements through calibrated wood and/or acrylic gages, a complete comparison was not made. It was intended that the work completed in this appendix would be available to subsequent researchers who will be able to accomplish the goals set out in Section 4. Separate model analysis was completed for the building in its entirety as shown in Figure A.11, and an individual building frame as shown in Figure A.12.

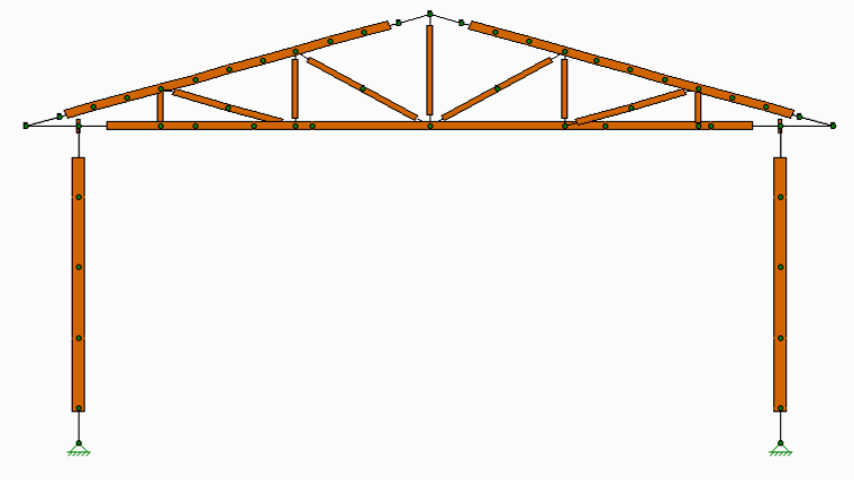

Fig. A.12. A model of an individual building frame as analyzed.

A.3 Results and Discussion

A.3.1 Frame

The results for the analysis of an individual frame indicate that the maximum compression force and bending moment for the posts are 26.1 kN and 3.7 kN·m, respectively. Figures A.13 a, b, and c and show the loads acting on the frame and figure A.13 d shows an exaggerated deflected shape of the frame.

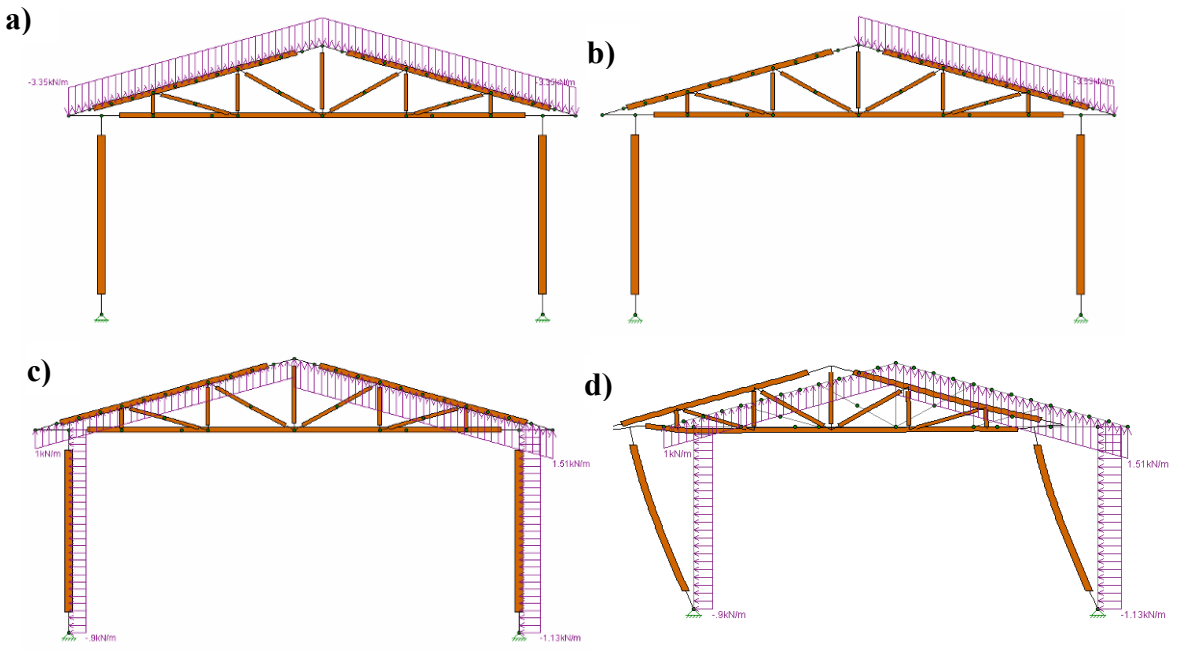

Fig. A.13. a) Snow load case I as analyzed on a frame. b) Snow load case II as analyzed on a frame. c) Wind load as analyzed on a frame. d) Deflected shape of frame under load.

Figure A.14 is a reproduction of the detailed structural performance report that is produced by RISA-3D for each building member. Each chart and graph shown in Fig. A.14 is interactive and can be used to determine the precise magnitude of each property at all locations on the member.

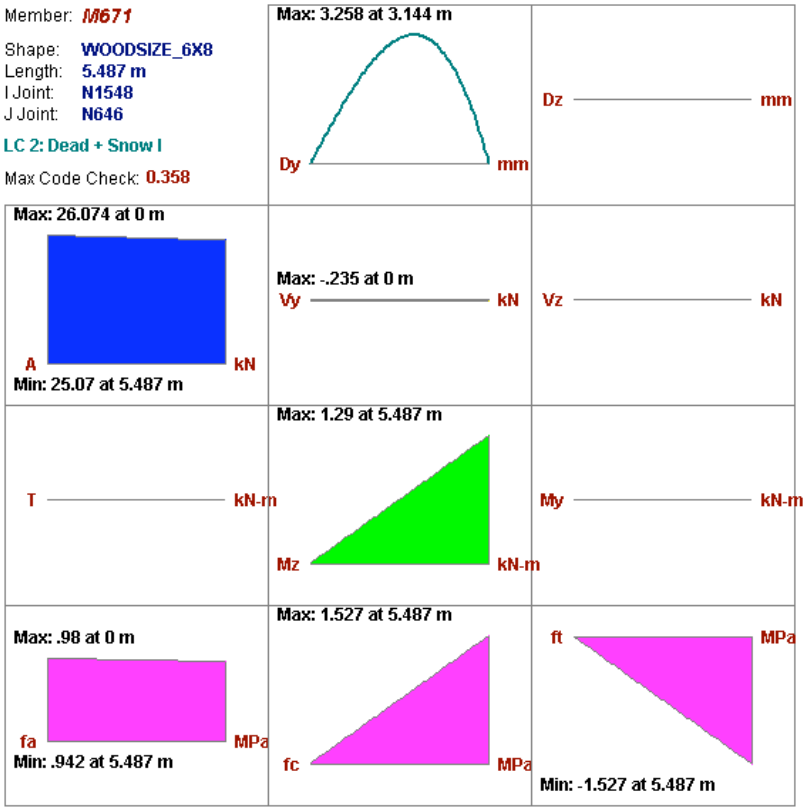

Fig. A.14. A reproduction of the graphical representation of the physical properties of each building member.

Figure A.15 is a reproduction of the code compliance analysis that RISA-3D produces for each building member. The chart indicates whether or not the member's structural performance complies with regulatory requirements.

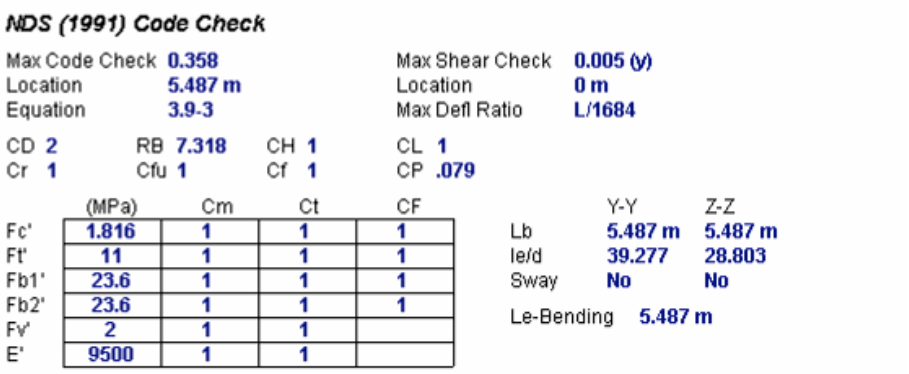

NDS (1991) Code Check

Max Code Check	0.358		Max Shear Check	0.005 (y)
Location	5.487 m		Location	0 m
Equation	3.9-3		Max Defl Ratio	L/1684

CD 2	RB 7.318	CH 1	CL 1
Cr 1	Cfu 1	Cf 1	CP .079

	(MPa)	Cm	Ct	CF
Fc'	1.816	1	1	1
Ft'	11	1	1	1
Fb1'	23.6	1	1	1
Fb2'	23.6	1	1	1
Fv'	2	1	1	
E'	9500	1	1	

	Y-Y	Z-Z
Lb	5.487 m	5.487 m
le/d	39.277	28.803
Sway	No	No

Le-Bending 5.487 m

Fig. A.15 The code compliance analysis completed by RISA-3D for each building member.

A.3.2. Post-Frame Building

The results for the analysis of the entire building indicate that the maximum compression force and bending moment for the posts are 56.4 kN and 10.9 kN·m, respectively. Figure A.16 shows the various loads considered for analysis of the entire building, and the buildings deflected shape under loading.

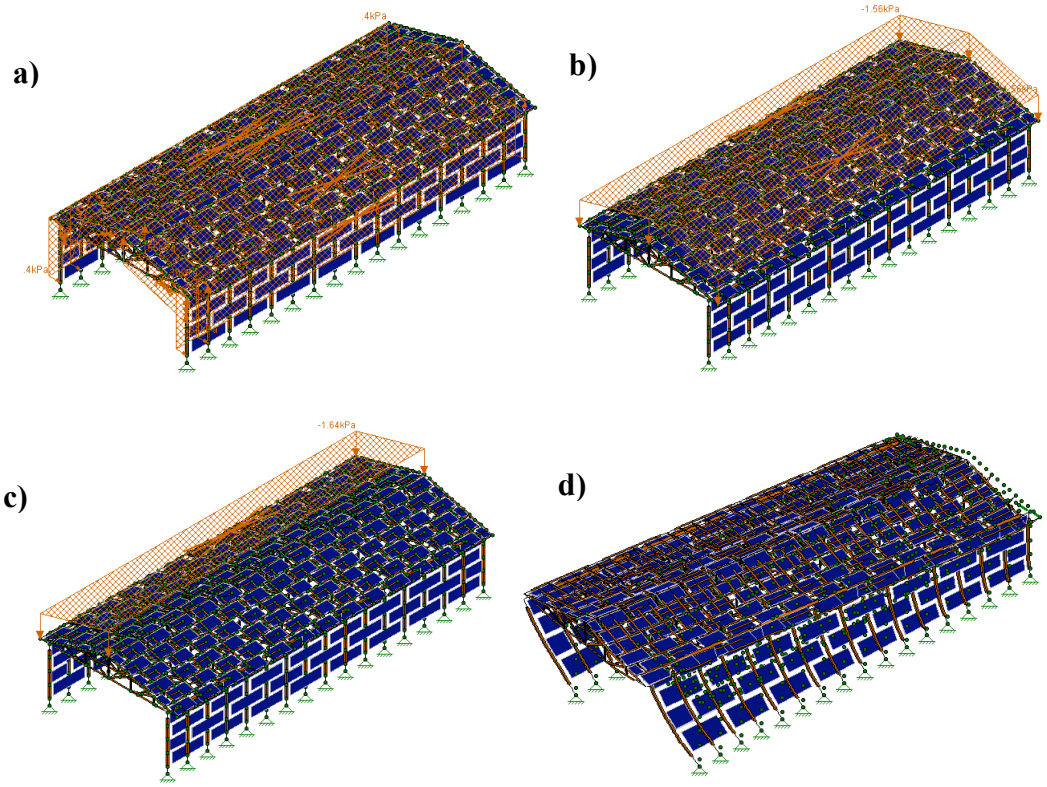

Fig. A.16.a) Wind load as analyzed on the entire building. b) Snow load case I as analyzed on the entire building. c) Snow load case II as analyzed on the entire building. d) Deflected shape of loaded building.

The model results for the post-frame building are different than the results obtained from the model of an individual post. This is likely due to the effects of the other structural

members on the post, including some level of moment transfer. Inadequately prescribed boundary and member end conditions are other probable factors influencing the results. For example, truss plates at truss member joints are most accurately modelled as spring connections, whereas for the sake of expediency and efficiency of analysis in this exercise most joints were modelled as pinned connections.

In both cases the experimental model does not give results consistent with the observed behaviour of post-frame buildings. This is likely due to the model's failure to properly account for diaphragm action and the positive influence of the interior and exterior stucco finishes performing as shear walls. It has become necessary to refine traditional experimental techniques to accommodate the design intricacies of post-frame buildings so that their design and construction can be accomplished with reasonable efficiencies.

The complex nature of the structural relationships between various elements of light-framed buildings causes uncertainties in predicting their performance, and necessitates assumptions of a conservative nature. Therefore, it is necessary to develop competent non-destructive evaluation techniques that can monitor the performance of light-framed structures under various loading conditions in order to increase the reliability and accuracy of design calculations and predictive modelling.

A.4 Conclusions

Structural modelling allows one to predict the behaviour of structures under various loading conditions. The ongoing advances in computer technology have increased the accuracy and reliability of structural models and has increased the complexity of the models that are able to be analyzed. Structural modelling software programs are powerful tools that can allow one to quickly test the performance of various design materials and configurations, decreasing the time that it takes to arrive at the optimum solution.

Current structural models are based on generally accepted structural analysis techniques. In nearly all cases this is completely appropriate, but in the field of structural engineering using biological materials some of the assumptions inherent in the computer code of the model do not adequately consider the benefits of this type of construction. One such scenario is the case of post-frame buildings. An analysis of an existing post-frame building was completed both through conventional on paper design calculations and through a commercially available structural modelling software program. This type of conventional structural analysis indicated that the design of the post-frame building may not be capable of withstanding the applied loads.

However the application of system analysis and the incorporation of diaphragm action into the design process as established by Bohnhoff (1990, 1992) and Anderson (1992) can result in a more efficient building design and prove the suitability of typical post-frame building designs. Within light-frame building design the relationships and

connections between different building members can be considered and applied to enhance building performance. New or revised software that is capable of modelling this type of performance is required.

In this report the predictive structural analysis focused on the performance of the post and determined that the compressive resistance of the post was 39.5 kN, but that the compressive force applied to the post was 26.2 kN. The calculated bending moment of 8.3 kN·m experienced by the post was less than the bending resistance of 10.2 kN·m. The modelling exercise determined a maximum compressive force of 56.4 kN and a maximum bending moment of 10.9 kN·m. The results of this study indicate a strong need for revisions to the analysis techniques for post-frame buildings. In order to determine what these revisions should entail, more accurate measurements of the structural performance of post-frame buildings are required.

APPENDIX B

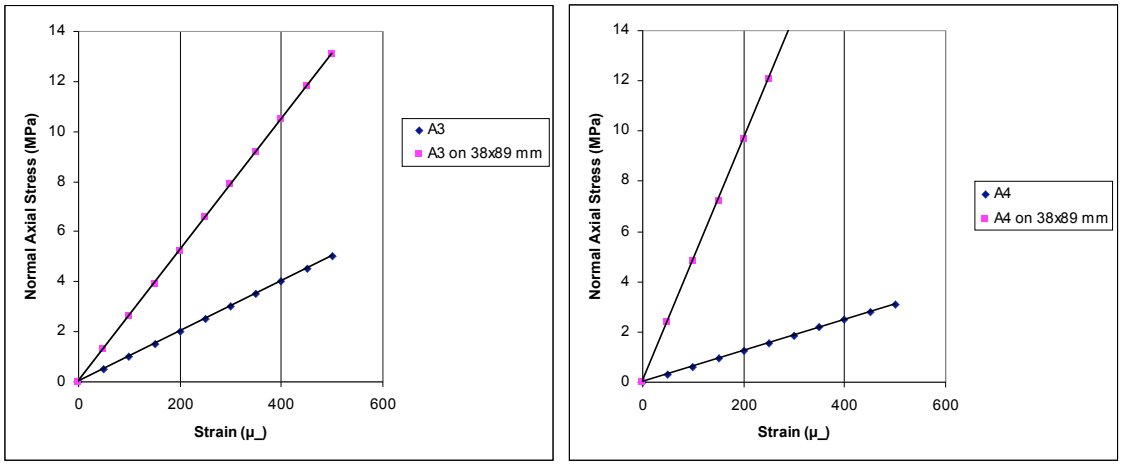

Fig. B.1. The slope variation between the calibration and structural phase of Treatment A

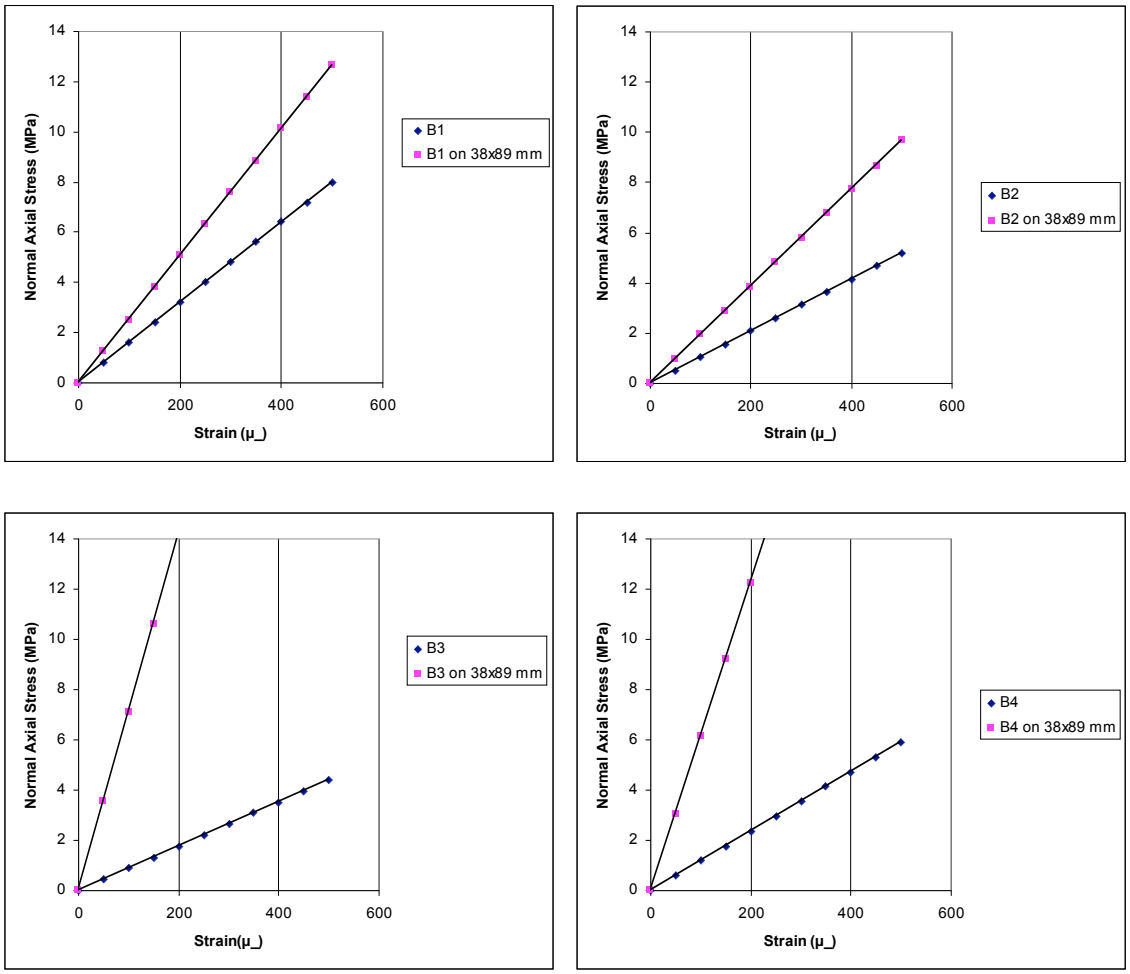

Fig. B.2. The slope variation between the calibration and structural phase of Treatment B